HELSINKI UNIVERSITY OF TECHNOLOGY

Department of Electrical and Communications Engineering

Olli Mäkelä

PARAMETER ESTIMATION FOR A SYNCHRONOUS MACHINE

Master's thesis submitted in partial fulfillment of the requirements for the degree of Master of Science in Technology

Espoo 17.8.2007

Supervisor

Professor Antero Arkkio

Instructor

M.Sc. Anna-Kaisa Repo

HELSINKI UNIVERSITY OF TECHNOLOGY Abstract of the Master's thesis

Author:	Olli Mäkelä	
Name of the work:	Parameter estimation for a synchronous machine	
Date:	17.8.2007	Number of pages: 45
Department:	Department of Electrical and Communications Engineering	
Professorship:	S-17 Electromechanics	
Supervisor:	Professor Antero Arkkio	
Instructor:	M.Sc. Anna- Kaisa Repo	

The aim of this study is to estimate two-axis model parameters for a synchronous machine using the numerical impulse method. An advantage of the numerical impulse method over the standstill frequency response and the sudden short circuit tests is that the obtained parameters describe behavior of the machine at the certain operation point. The operation point may be a loaded operation point with a three-phase supply.

The parameters of the machine have been estimated using data from linear and nonlinear finite element models. It is seen that saturation does not affect much when an impulse with the amplitude of 1% of the average RMS-value of the line voltages is used.

A linearization method based on the Taylor's expansion is presented for synchronous machine equations. In addition, a computationally effective way to establish transfer functions is presented. The transfer function derivation takes advantage of the linear system representation and states of the system.

Stability issues concerning the circuit model have been investigated in the sense of Lyapunov. It is taken note that there is only one steady state. The effect of the impulse amplitude in the non-linear FEM model has been studied by doing different impulse sizes and the frequency responses are compared.

The numerical impulse response method is verified using circuit simulations in Simulink. The frequency responses obtained from circuit simulations, with the estimated parameters, match well with the frequency responses of finite element simulations. The similarity verifies the used methods and the applicability of the numerical impulse method in parameter estimation.

Keywords: parameter estimation, synchronous machine, numerical impulse method, frequency response

TEKNILLINEN KORKEAKOULU Diplomityön tiivistelmä

Tekijä:	Olli Mäkelä	
Työn nimi:	Tahtikoneen parametrien estimointi	
Päivämäärä:	17.8.2007	Sivumäärä: 45
Osasto:	Sähkö- ja tietoliikennetekniikan osasto	
Professuuri:	S-17 Sähkömekaniikka	
Työn valvoja:	Professori Antero Arkkio	
Työn ohjaaja:	DI Anna- Kaisa Repo	

Tämän työn tavoitteena on estimoida tahtikoneen kaksiakselimallin parametrit käyttäen numeerista impulssimenetelmää. Esitetyn menetelmän etu on, että saadut parametrit kuvaavat todellista toimintapistettä, toisin kuin harmonisen taajuusanalyysin ja oikosulkukokeen avulla saadut parametrit.

Tahtikoneen parametrit on arvioitu käyttäen lineaarista ja epälineaarista elementtimenetelmämallia. Huomataan, että kyllästyminen ei juuri vaikuta taajuusvasteisiin, kun käytetään 1 % verkkojännitteen RMS-arvon suuruista impulssia.

Työssä esitetään Taylorin kehitelmään perustuva lineaarisointimenetelmä tahtikoneen yhtälöille. Lisäksi esitetään laskennallisesti tehokas menetelmä siirtofunktion muodostamiseen, jossa käytetään lineaarisen systeemin esitystä ja tiloja hyväksi.

Piirimallille on suoritettu stabiilisuustarkastelu Lyapunovin mielessä. Todetaan, että systeemillä on vain yksi pysyvä tila. Syötetyn impulssin amplitudin suuruuden vaikutusta taajuusvasteeseen elementtimenetelmän epälineaarisessa mallissa tutkitaan käyttämällä erisuuruisia impulsseja.

Numeerisen impulssimenetelmän toimivuus on osoitettu todeksi piirimallilla tehtyjen simulaatioiden avulla Simulink- ympäristössä. Piirimallissa on käytetty estimoituja parametreja. Piirimallilla tehtyjen simulaatioiden taajuusvasteet vastasivat hyvin FEM simulaatioilla saatuja taajuusvasteita. Taajuusvasteiden yhteneväisyys osoittaa todeksi käytetyt menetelmät ja numeerisen impulssimenetelmän käyttökelpoisuuden parametrien estimoinnissa.

Avainsanat: parametrien estimointi, tahtikone, numeerinen impulssimenetelmä, taajuusvaste

Foreword

This work has been carried out in the Laboratory of Electromechanics at Helsinki University of Technology, TKK, during the spring and summer 2007. I would like to thank my instructor Anna-Kaisa Repo and supervisor Antero Arkkio for advices, comments and help during this study.

I would also like to thank Jarmo Perho, Marko Hinkkanen and Mikaela Cederholm for instructive discussions we had during my project. Additionally, I thank Jan Westerlund from ABB Oy for providing data of the studied machine.

Finally, I would like to thank my parents, siblings and friends for support during my studies.

In Otaniemi, August 2007

Olli Mäkelä

Contents

Symbols and acronyms

Symbols

e	error
f	frequency
G	transfer function
i	current
I	inertia
j	complex variable
J	rotation matrix
L	inductance of an inductor
p	number of pole pairs
P	power
R	resistance of a resistor
s	Laplace operator
t	time
T	torque
u	voltage
Y	admittance
Z	impedance

Greek symbols

Δ	deviation
ψ	flux
ω	angular frequency
Ω	mechanical speed

Subscripts

0	operation point
B	base value
d	direct axis
D	direct axis damper winding
e	electrical
f	field winding
imp	impulse
m	mechanical

mr	mutual component in rotor
ms	mutual component in stator
q	quadrature axis
Q	quadrature axis damper winding
r	rotor
rel	relative amplitude
rms	root mean square
s	stator

Acronyms

DE	Differential Evolution
FE	finite element
FEA	finite element analysis
FEM	finite element method
MIMO	multiple input multiple output
p. u.	per unit
SSFR	stand still frequency response

1 Introduction

This master's thesis deals with parameter estimation for a synchronous machine. A conventional two-axis circuit model is adequate for many applications, provided the parameters are properly defined. The aim of this study is to introduce new sights in parameter estimation against previous and conventional methods.

The appropriate parameter values are essential in control design and in power system applications. With accurate parameter values, the behavior of a machine can be predicted well.

Nowadays, finite element analysis (FEA), Bastos, J. P. A. et al. (2003), is the state of the art in electrical machine design. The FEA gives accurate results, and in that perspective, it is natural that parameter estimation process using FEA would be a good approach in order to get competent parameter values.

In this study, the numerical impulse method is applied in FEA and parameter values are extracted from finite element (FE) data, Figure 1. The impulse and the response together form a numerical transfer function. An analytical transfer function based on a conventional two-axis circuit model is derived and it is fitted into the numerical transfer function. The best fit gives the parameter values.

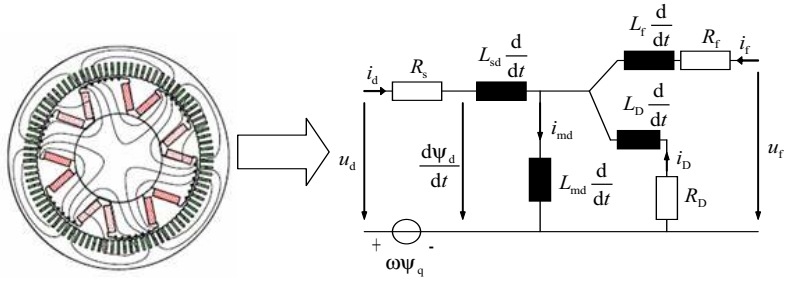

Figure 1 Purpose of the work. The parameters of the equivalent circuit are obtained from finite element analysis.

1.1 Literature review

The impulse response test has long traditions in mechanics. The method is used for fault diagnosis. In the method, a hammer is used to create an impulse, and the vibration response is recorded. From the vibration response the faults can be diagnosed. The impulse method is also applied successfully in research of magnetic forces generated by eccentric rotor, studied by Tenhunen A. (2003), Holopainen T. (2004) and Burakov A. et al. (2006).

An idea of using the numerical impulse method in FEA to estimate the parameters of an equivalent circuit is not widely studied. However, Repo A.-K. et al. (2006a, 2006b & 2007) have studied these issues for induction machines in three papers. The idea behind the impulse response test is to apply an excitation, which includes many frequencies. Thus we can avoid the usage of the harmonic excitation that means supplying one excitation frequency at a time.

There are no publications studying this method for synchronous machines. Therefore the aim of this study is also to check the applicability of this method for synchronous machines.

The Institute of Electrical and Electronics Engineers (IEEE) (1995) presents guidelines for parameter estimation for a synchronous machine. There are also publications written, for example, by Keyhani, A. et al. (1994) and Bortoni, E. C. et al. (2004), about parameter estimation for synchronous machines using standstill frequency response (SSFR). In the SSFR, it is assumed that the resistance of windings is determined by other means and the machine is tested over a certain frequency range. The armature or the field winding is supplied from a single-phase variable-frequency supply. Using monitored values of voltages and currents, the variation of the modulus and phase angle of the operational impedance are obtained. Operational impedance curves can be used to obtain parameters of a synchronous machine.

A widely known way to estimate dynamical parameters of the synchronous machine is the use of a sudden three-phase short-circuit test presented, for example, by Wamkeue, R. Kamwa, I. et al. (2003). In this method, an unloaded generator is driven at the rated speed and the field voltage is maintained constant during the test. A short-circuit is caused. The line voltage and short-circuit current are recorded by voltage and current transformers. The dynamic reactances and time-constants may be computed from the response.

The advantage of the proposed method is that it may be used at a certain operation point, and the obtained parameters describe the behavior at that point well. In the SSFR test, the rotor is at stand still and therefore it does not give appropriate parameters for an operation point where the rotor is rotating.

1.2 Fundamental properties of electrical machines

In this study, the parameters are estimated for a synchronous machine. An electrical machine converts electrical energy into mechanical energy in a motor, or vice versa in generator operation. The conversion process is not perfect because of the losses heat,

noise, etc., Figure 2. Despite the losses, the efficiency of a synchronous machine is quite high and it is higher than in induction machines. The high efficiency is a reason for synchronous machine usage in power systems and in high power drives.

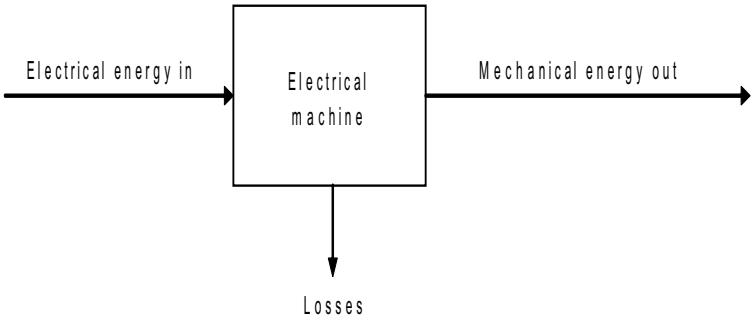

Figure 2 Energy flow in an electrical machine in motor operation. An electrical motor converts electrical energy to mechanical energy via magnetic field. The conversion process is not perfect, and therefore there are some losses.

1.3 Two axis model of synchronous machines

A conventional three phase synchronous machine consists of a rotor and stator. The rotor and stator bodies are made of highly permeable material. The stator has a three-phase winding, and the rotor has an excitation winding, which is supplied by DC current. In the two-axis model in Figure 3, the rotor has also two damper windings.

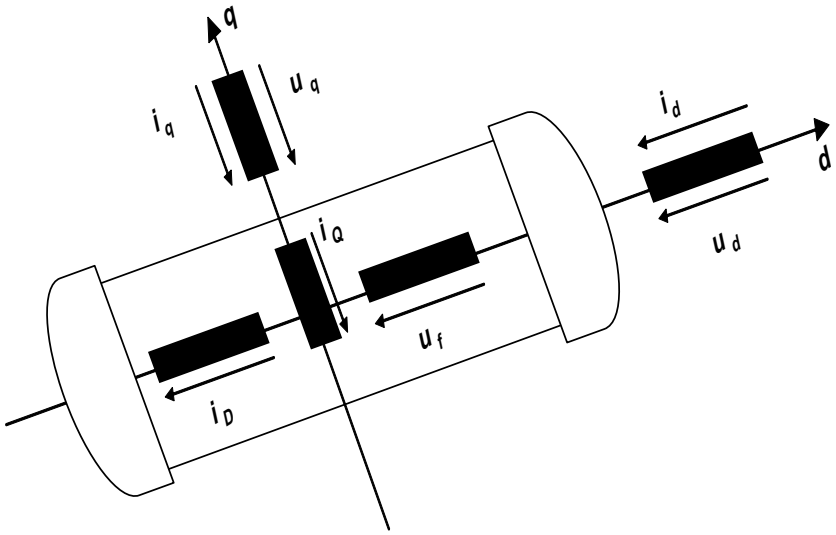

Figure 3 Two-axis model of the synchronous machine.

In Figure 3, u_q, u_d, u_f are the quadrature axis, direct axis and field winding voltage, respectively. i_Q and i_D are the quadrature and direct axis damper winding currents.

1.4 Elementary properties of synchronous machines

A synchronous machine is often started as a conventional induction machine on its damper winding. The field voltage is turned on afterwards, when the machine has almost reached its synchronous speed.

The synchronous speed depends on the number of poles and the frequency of voltage source. The speed is defined as follows

$$\Omega_{\mathrm{m}} = \frac{2\pi f}{p} \tag{1}$$

where, p is the number of pole pairs and f denotes the frequency of the voltage source.

In steady state operation, there is no current flow in the damper windings. The rotating speed is the synchronous speed.

1.5 Per-unit notation

The per-unit notation may be conceptually helpful in the analysis of synchronous machines. Using the notation makes the parameters of all machines become quite similar. For variables a base value is noted, and then the variable is divided by its base value. In other words, per-unit notation is a way to normalize a machine. Normally, the base value is wanted to tie to some aspect of normal operation, to machine ratings for instance.

The normalizing process covers the voltage, current, power, torque, flux and impedance. In fact, only the base voltage U_{B}, current I_{B} and frequency ω_{B} have to be specified. Having done this, other base quantities can be derived.

Variable	Formula
Base power	$P_{\mathrm{B}} = \frac{3}{2} U_{\mathrm{B}} I_{\mathrm{B}}$
Base flux	$\psi_{\mathrm{B}} = \frac{U_{\mathrm{B}}}{\omega_{\mathrm{B}}}$
Base torque	$T_{\mathrm{B}} = \frac{p}{\omega_{\mathrm{B}}} P_{\mathrm{B}}$
Base impedance	$Z_{\mathrm{B}} = \frac{U_{\mathrm{B}}}{I_{\mathrm{B}}}$

2 Methods

2.1 Simulation model

The use of the two-axis model is a conventional way to simulate synchronous machines. The idea behind the model is to divide all variables into two axes. They are perpendicular to each other, and therefore, there is no interaction. The rotor of a salient-pole synchronous machine is asymmetric, and therefore equations are considered in a system, which is rotating at rotor speed. Commonly, quantities, such as voltages and currents, are referred to the stator.

The synchronous machine operation, in a conventional two-axis model, may be described properly with five voltage equations and a torque equation. In addition, we need five flux-linkage equations. The system of equations is nonlinear, and therefore it can only be solved completely using numerical methods.

The five voltage equations are presented below. They are referred to the stator and they are in a reference frame, which is rotating at electrical angular speed of the rotor ω_r.

$$u_\mathrm{d} = R_\mathrm{s} i_\mathrm{d} + \frac{\mathrm{d}\psi_\mathrm{d}}{\mathrm{d}t} + \omega_\mathrm{r}\psi_\mathrm{q} \tag{2}$$

$$u_\mathrm{q} = R_\mathrm{s} i_\mathrm{q} + \frac{\mathrm{d}\psi_\mathrm{q}}{\mathrm{d}t} + \omega_\mathrm{r}\psi_\mathrm{d} \tag{3}$$

$$0 = R_\mathrm{D} i_\mathrm{D} + \frac{\mathrm{d}\psi_\mathrm{D}}{\mathrm{d}t} \tag{4}$$

$$u_\mathrm{f} = R_\mathrm{f} i_\mathrm{f} + \frac{\mathrm{d}\psi_\mathrm{f}}{\mathrm{d}t} \tag{5}$$

$$0 = R_\mathrm{D} i_\mathrm{D} + \frac{\mathrm{d}\psi_\mathrm{D}}{\mathrm{d}t} \tag{6}$$

The system of equations can be represented in matrix form, as below, by separating the stator and rotor voltage equations

$$\frac{\mathrm{d}\psi_\mathrm{s}}{\mathrm{d}t} = u_\mathrm{s} - R_\mathrm{s} i_\mathrm{s} - \omega_\mathrm{k} J_\mathrm{s} \psi_\mathrm{s} \tag{7}$$

$$\frac{\mathrm{d}\psi_\mathrm{r}}{\mathrm{d}t} = u_\mathrm{r} - R_\mathrm{r} i_\mathrm{r} \tag{8}$$

where

$$\psi_s = \begin{bmatrix} \psi_d \\ \psi_q \end{bmatrix} u_s = \begin{bmatrix} u_d \\ u_q \end{bmatrix} R_s = \begin{bmatrix} R_d & 0 \\ 0 & R_q \end{bmatrix} i_s = \begin{bmatrix} i_d \\ i_q \end{bmatrix} i_s = \begin{bmatrix} i_d \\ i_q \end{bmatrix} J_s = \begin{bmatrix} 0 & -1 \\ 1 & 0 \end{bmatrix}$$

and

$$\psi_r = \begin{bmatrix} \psi_f \\ \psi_D \\ \psi_Q \end{bmatrix} u_r = \begin{bmatrix} u_f \\ 0 \\ 0 \end{bmatrix} R_r = \begin{bmatrix} R_f & 0 & 0 \\ 0 & R_D & 0 \\ 0 & 0 & R_Q \end{bmatrix} i_r = \begin{bmatrix} i_f \\ i_D \\ i_Q \end{bmatrix}$$

The flux linkages may also be separated to stator and rotor matrices

$$\psi_s = L_s i_s + L_{mr} i_r \tag{9}$$

$$\psi_r = L_{ms} i_s + L_r i_r \tag{10}$$

where

$$L_s = \begin{bmatrix} L_{sd} & 0 \\ 0 & L_{sq} \end{bmatrix}$$

$$L_{mr} = \begin{bmatrix} L_{md} & L_{md} & 0 \\ 0 & 0 & L_{mq} \end{bmatrix}$$

$$L_r = \begin{bmatrix} L_f & 0 & 0 \\ 0 & L_D & 0 \\ 0 & 0 & L_Q \end{bmatrix}$$

$$L_{ms} = \begin{bmatrix} L_{md} & 0 \\ L_{md} & 0 \\ 0 & L_{mq} \end{bmatrix}$$

These can be rewritten

$$\psi = Li$$

where

$$L = \begin{bmatrix} L_s & L_{mr} \\ L_{ms} & L_r \end{bmatrix} = \left[\begin{array}{cc|ccc} L_{sd} & 0 & L_{md} & L_{md} & 0 \\ 0 & L_{sq} & 0 & 0 & L_{mq} \\ \hline L_{md} & 0 & L_f & 0 & 0 \\ L_{md} & 0 & 0 & L_D & 0 \\ 0 & L_{mq} & 0 & 0 & L_Q \end{array}\right]$$

The torque equation is

$$\frac{J}{p}\frac{\mathrm{d}\omega}{\mathrm{d}t} = T_\mathrm{e} + T_\mathrm{m} \tag{11}$$

The conventional equivalent circuits following the two-axis model, according to Luomi et. al. (2005), are below.

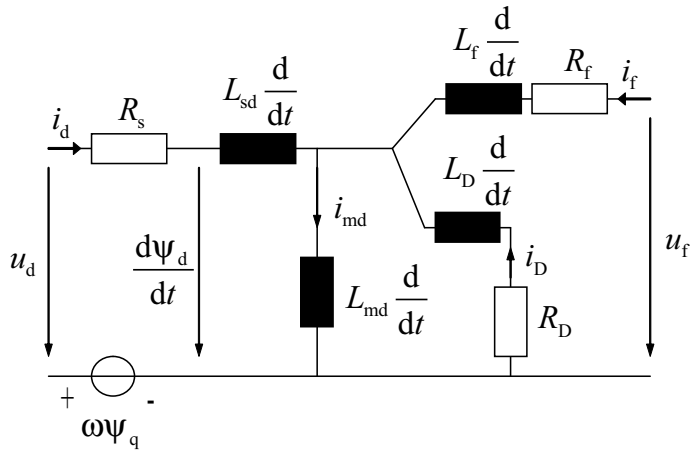

Figure 4 Standard two-axis model equivalent circuit of the d-axis of the synchronous machine.

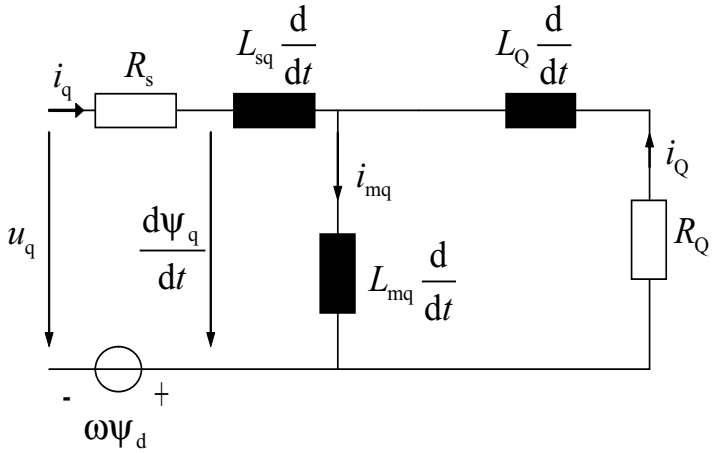

Figure 5 Standard two-axis model equivalent circuit of the q-axis of the synchronous machine.

2.2 MIMO- representation

When using the two-axis model in the analysis of synchronous machines, there are two inputs, namely u_d and u_q. There are also two outputs, i_d and i_q. This kind of system is called the MIMO (Multiple Input Multiple Output) –system, Figure 6. Therefore we should consider the machine as an MIMO-system with two inputs and two outputs. In the MIMO representation, the transfer function is a 2x2 matrix.

Figure 6 Schematic diagram of an MIMO system. In the MIMO-model, there may be many inputs and many outputs. In this representation, the transfer function is a matrix.

We may define a 2x2 transfer function matrix, which is an admittance matrix if the voltage is considered as the input.

$$\begin{bmatrix} \Delta i_{\mathrm{d}} \\ \Delta i_{\mathrm{q}} \end{bmatrix} = \begin{bmatrix} Y_{11} & Y_{12} \\ Y_{21} & Y_{22} \end{bmatrix} \begin{bmatrix} \Delta u_{\mathrm{d}} \\ \Delta u_{\mathrm{q}} \end{bmatrix} \tag{12}$$

In order to define the admittance matrix, the numerical impulse test is performed. Two FEM simulations with perpendicular impulses and a FEM simulation without any impulse are run, first to u_{d} while $u_{\mathrm{q}} = 0$, and then to u_{q} while $u_{\mathrm{d}} = 0$. The perpendicular impulses with the simulation without impulse determine the elements Y_{11}, Y_{12}, Y_{21} and Y_{22}. An impedance matrix is an inverse of the admittance matrix.

2.3 Order of the two-axis model

The basic two-axis model in Figure 4 has the order of two. One way, which may improve success in the fit, is to increase the order of the model, Keyhani, A. et al. (1994). The higher is the order of the model; the better is the fit. In the two-axis model it would mean that we add a new voltage equation, a new damper winding for instance. The additional damper winding can also be modeled in the circuit model. In Figure 7, the additional damper winding is depicted with a striped box. However, usually we want to preserve the standard two-axis model without modification.

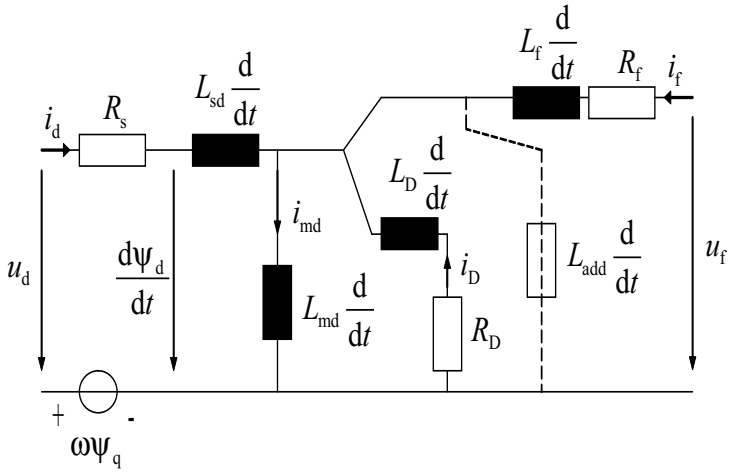

Figure 7 Additional damper winding. It increases the order of the model.

2.4 Linearization of the set of equations

The set of equations of synchronous machines is nonlinear. However, a good model regarding small-displacement behavior about an operation point may be achieved by linearizing the equations. Since the machine can be treated as a linear system, the eigenvalues can be calculated and transfer functions can be established based on linear system theory. For instance, Glad, T. et al. (2000) presented the theory of the system linearization.

A nonlinear equation system may be presented as below

$$\begin{cases} \begin{bmatrix} \dot{x}_1 \\ \dot{x}_2 \\ \vdots \\ \dot{x}_n \end{bmatrix} = \begin{bmatrix} f_1(x(t),u(t)) \\ f_2(x(t),u(t)) \\ \vdots \\ f_n(x(t),u(t)) \end{bmatrix} \\ y(t) = g(x(t),u(t)) \end{cases} \tag{13}$$

The displacement variables can be presented in form

$$\begin{cases} \Delta x(t) = x(t) - x_0(t) \\ \Delta u(t) = u(t) - u_0(t) \\ \Delta y(t) = y(t) - y_0(t) \end{cases}$$

where subscript 0 refers to the operation point and Δf is the displacement.

The linear state-space presentation for displacements is

$$\begin{cases} \Delta \dot{x}(t) = A\Delta x(t) + B\Delta u(t) \\ \Delta y(t) = C\Delta x(t) + D\Delta u(t) \end{cases} \tag{14}$$

The system matrix is defined, as below,

$$A = \begin{bmatrix} \frac{\mathrm{d}f_1(x,u)}{\mathrm{d}x_1} & \frac{\mathrm{d}f_2(x,u)}{\mathrm{d}x_2} & \cdots & \frac{\mathrm{d}f_1(x,u)}{\mathrm{d}x_n} \\ \frac{\mathrm{d}f_2(x,u)}{\mathrm{d}x_1} & \frac{\mathrm{d}f_2(x,u)}{\mathrm{d}x_2} & \cdots & \frac{\mathrm{d}f_2(x,u)}{\mathrm{d}x_n} \\ \vdots & & \ddots & \vdots \\ \frac{\mathrm{d}f_n(x,u)}{\mathrm{d}x_1} & \frac{\mathrm{d}f_n(x,u)}{\mathrm{d}x_1} & \cdots & \frac{\mathrm{d}f_n(x,u)}{\mathrm{d}x_n} \end{bmatrix}$$

The input matrix is

$$B = \begin{bmatrix} \frac{\mathrm{d}f_1(x,u)}{\mathrm{d}u} \\ \frac{\mathrm{d}f_2(x,u)}{\mathrm{d}u} \\ \vdots \\ \frac{\mathrm{d}f_\mathrm{n}(x,u)}{\mathrm{d}u} \end{bmatrix}$$

The output matrix is

$$C = \begin{bmatrix} \frac{\mathrm{d}g(x,u)}{\mathrm{d}x_1} & \frac{\mathrm{d}g(x,u)}{\mathrm{d}x_2} & \cdots & \frac{\mathrm{d}g(x,u)}{\mathrm{d}x_\mathrm{n}} \end{bmatrix}$$

and the transmission matrix

$$D = \frac{\mathrm{d}g(x,u)}{\mathrm{d}u}$$

This formulation might be more practical than the one presented by Müller, G. (1985). This approach does not need substitution of variables by their linear approximations, but it takes advantage of the Taylor's expansion.

After the linearization, a linear state-space representation for a synchronous machine can be obtained. Flux linkages have been chosen as the state variables.

The state-space form for the stator voltage perturbation investigation is

$$\frac{\mathrm{d}\Delta x}{\mathrm{d}t} = A\Delta x + B_\mathrm{s}\Delta u_\mathrm{s} \tag{15}$$

The system matrix is

$$A = -\begin{bmatrix} R_\mathrm{s} & 0 \\ 0 & R_\mathrm{r} \end{bmatrix} L^{-1} - \begin{bmatrix} \omega_\mathrm{k} J_\mathrm{s} & 0 \\ 0 & (\omega_\mathrm{k} - \omega_\mathrm{m}) J_\mathrm{r} \end{bmatrix}$$

The state-vector is

$$x = \begin{bmatrix} \psi_\mathrm{s} \\ \psi_\mathrm{r} \end{bmatrix} \tag{16}$$

The input matrix is

$$B_\mathrm{s} = \begin{bmatrix} I \\ 0 \end{bmatrix}$$

I is a 2x2 identity matrix, and 0 is a 3x2 zero matrix.

2.5 Stability analysis

The eigenvalues of the system matrix A describe machine's stability properties at the linearization point. If the eigenvalues are on the left half plane, the system will return to its stationary state after a small perturbation and the system is stable. Eigenvalues on the right half plane mean that the system is unstable.

However, an unstable system may be stabilized using feedback. The original system is still unstable, but the whole system, which consists of the original system and the feedback, may be stable. Therefore, the response does not grow towards infinity.

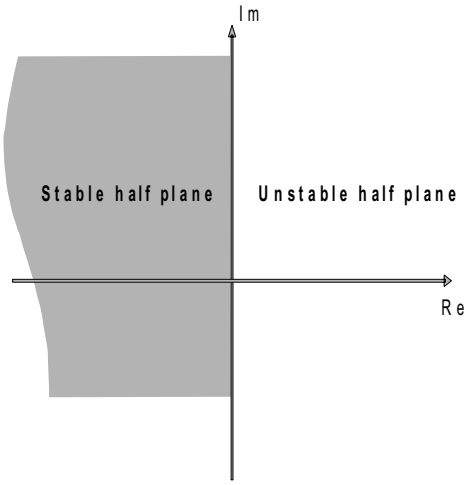

Figure 8 Left and right half plane indicate stable and unstable area, respectively. If there is any pole on the unstable half plane, the system is unstable. Otherwise, the system is stable.

2.5.1 Stability with respect to impulse size in the circuit model

The impulse size, which can be applied in the stator voltage, may be restricted when the two-axis circuit model is used. The issue concerning the impulse size may be investigated using Lyapunov-stability analysis, presented, for example, by Glad, T. et al. (2000) and Struble, R. A. (1962).

The Lyapunov function is a way to investigate stability. The idea is that a function $V(x)$ could be found with the following properties.

$$V(x_0) = 0 \tag{17}$$

$$V(x) > 0\,,\ x \neq x_0 \tag{18}$$

$$\nabla V(x) f(x) < 0 \tag{19}$$

$f(x)$ is presented in Equation 13. An arbitrary point can be interpreted as a point at origin by making a coordinate transform. Therefore, the stability study at the origin is sufficient. At the origin, the input is zero.

One may consider stator voltage as the input. The voltage equation for the stator

$$\frac{\mathrm{d}}{\mathrm{d}t}\begin{bmatrix}\psi_\mathrm{d}\\ \psi_\mathrm{q}\end{bmatrix} = -R_\mathrm{s}\begin{bmatrix}i_\mathrm{d}\\ i_\mathrm{q}\end{bmatrix} - \omega_\mathrm{k}\begin{bmatrix}0 & -1\\ 1 & 0\end{bmatrix}\begin{bmatrix}\psi_\mathrm{d}\\ \psi_\mathrm{q}\end{bmatrix}$$

Using substitution $\begin{bmatrix}\psi_\mathrm{d}\\ \psi_\mathrm{q}\end{bmatrix} = \begin{bmatrix}x_1\\ x_2\end{bmatrix}$, the set of equations above may be formulated, as follows,

$$\begin{cases}\dot{x}_1 = -R_\mathrm{s}L_\mathrm{d}^{-1}x_1 + \omega_\mathrm{k}x_2\\ \dot{x}_2 = -R_\mathrm{s}L_\mathrm{q}^{-1}x_2 - \omega_\mathrm{k}x_1\end{cases}$$

We may try a Lyapunov function, which has the following form

$$V(x) = \alpha x_1^2 + x_2^2,\ \alpha > 0$$

then holds $V(x) > 0$, when $x \neq x_0$ and $V(x_0) = 0$ when $x = x_0 = 0$

$$\nabla V(x) = \begin{bmatrix}2\alpha x_1 & 2x_2\end{bmatrix}$$

$$\nabla V(x) f(x) = -2\alpha x_1 R_\mathrm{s}L_\mathrm{d}^{-1}x_1 + 2\alpha x_1\omega_\mathrm{k}x_2 - 2x_2R_\mathrm{s}L_\mathrm{q}^{-1}x_2 - 2x_2\omega_\mathrm{k}x_1$$

Choosing $\alpha = 1$ one gets

$$\nabla V(x) f(x) = -2R_\mathrm{s}L_\mathrm{d}^{-1}x_1^2 - 2R_\mathrm{s}L_\mathrm{q}^{-1}x_2^2 < 0$$

So, a valid Lyapunov function may be $V(x) = x_1^2 + x_2^2$. Its isolines are circles with the center at the origin. The circles have different radii, Figure 9. The system is stable inside the circle.

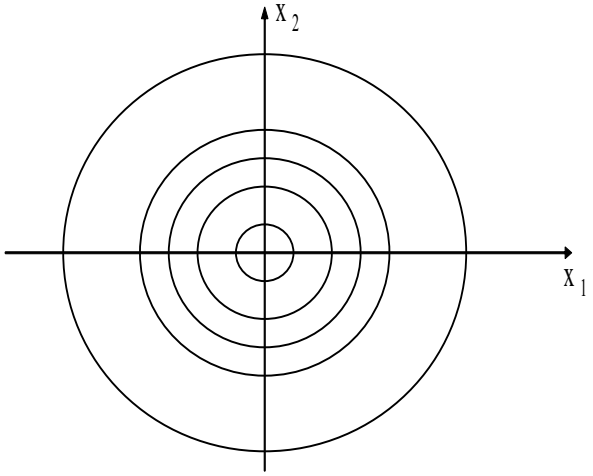

Figure 9 Isolines with different Lyapunov-function values. All the isolines have the same midpoint, and therefore there is only one steady state.

A system is globally asymptotically stable if there is a function V, additional to Eq. 17-19, satisfying

$$V(x) \to \infty, \text{ when } |x| \to \infty$$

If we are considering a circuit model, the impulse size does not affect to the operation point. There is only one steady state. The system is stable in the sense of Lyapunov, and the system will always return to its steady state. The return time depends on the eigenvalues of the system matrix. The further on the left half plane the eigenvalues are, the faster the machine returns to its steady state.

The analysis is tested with two impulses, which have the peak values 225 and 22500 voltages, Figure 10 and Figure 11. It can be noticed that deviations go towards zero in the both cases. The simulations are made with a circuit model, which is presented in Appendix 1.

Based on the results, it seems that the Lyapunov stability analysis holds well. In addition, the circuit model is globally stable and there is only one steady state. The result gives freedom to choose the impulse amplitude without any concern about loosing the operation point.

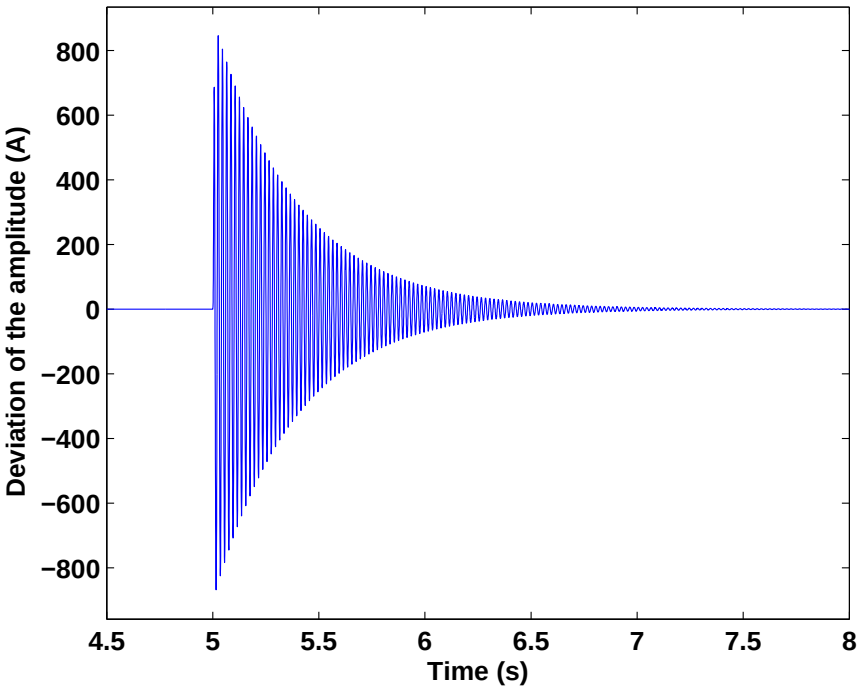

Figure 10 Current deviation caused a voltage impulse. The deviation, at different times, after applying an impulse with a peak value of 225 V. Deviation goes towards zero as time goes on.

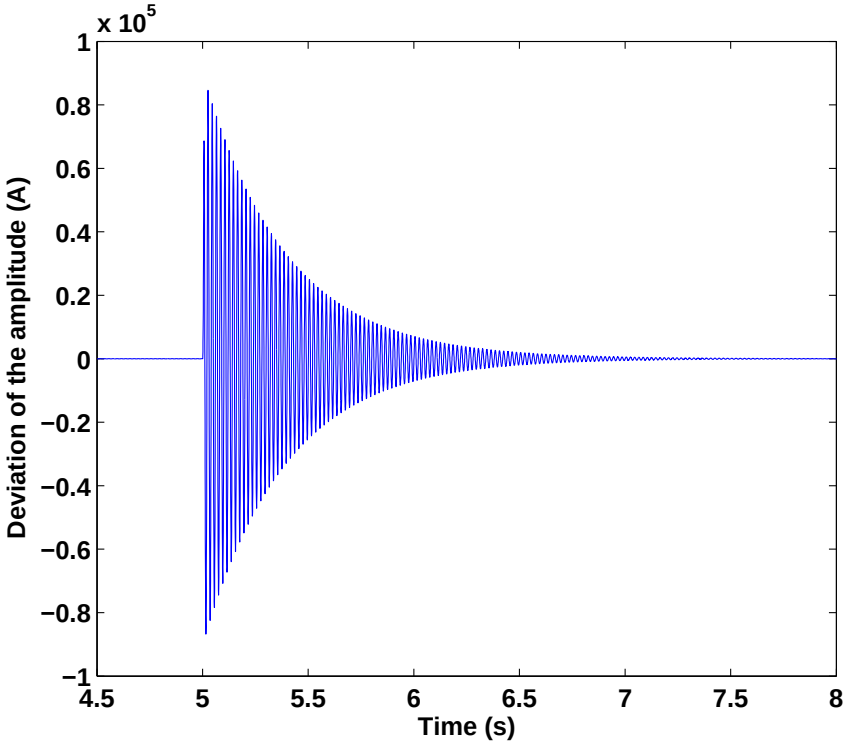

Figure 11 Current deviation caused a voltage impulse. In this case, the size of the impulse is 22500 voltages.

2.6 Theoretical transfer function formulation

The transfer function formulation is an essential part of the proposed method. The transfer function is fitted in the FEM data, and the parameters are obtained from the fit. A transfer function between two variables may be established from basic linear control theory. The linear system representation is

$$\begin{cases} \mathrm{s}x = Ax + Bu \\ y = Cx + Du \end{cases}$$

where x, u, s and y are the state vector, the input vector, the Laplace operator and the output vector, respectively. From the first equation, the input vector can be solved

$$x = (\mathrm{s}I - A)^{-1} Bu$$

and after the substitution into the second equation, we get

$$y = C(\mathrm{s}I - A)^{-1} Bu + Du$$

$D = 0$, since we consider $\dfrac{\mathrm{d}g(x,u)}{\mathrm{d}u} = 0$. If the stator current is considered as an output variable, the output vector can be selected as follows

$$y = i_s = \begin{bmatrix} i_d \\ i_q \end{bmatrix} = C_s x$$

where

$$C_s = \begin{bmatrix} I & 0 \end{bmatrix} L^{-1}$$

x is the state vector, $x = \begin{bmatrix} \psi_s \\ \psi_r \end{bmatrix}$

For instance, a transfer function between stator current and voltage may be presented as follows

$$i_s = Y_s u_s$$

$$Y_s(s) = C_s(sI - A)^{-1} B_s$$

where, $B_s = \begin{bmatrix} I \\ 0 \end{bmatrix}$

This kind of transfer function formulation is more efficient than the one presented by Krause et al. (2002). The formulation presented by Krause needs a matrix inversion for a 5x5 matrix three times, whereas the above formulation only once. Therefore, this approach is computationally more efficient.

2.7 Numerical transfer function

The numerical transfer function is established from the time-stepping FEM data. The purpose of the numerical transfer function is to give the estimation data for wherein the theoretical transfer function is fitted. Normally the transfer function is considered in frequency domain, and the Fourier transform makes the transformation from the time to frequency domain. In the frequency domain, the transfer function may be presented, as follows

$$G(\mathrm{j}\omega) = \frac{Y(\mathrm{j}\omega)}{U(\mathrm{j}\omega)}$$

$Y(\mathrm{j}\omega)$ and $U(\mathrm{j}\omega)$ are the input and output data in frequency domain, respectively. The transfer function $G(\mathrm{j}\omega)$ is also called the frequency response function. It depicts the spectral properties of the system.

The input should include all desired frequencies in order to take all time constants into account. Different inputs produce different outputs, but the ratio is always constant. The ratio is the numerical transfer function.

2.8 Effect of saturation in the sense of parameter estimation

In this study, three different models are considered. The two axis model is linear the speed is constant. The linear FE-model is also a linear model. The non-linear FE-model takes the saturation into account. Normally, saturation makes the behavior of the machine different compared to a linearized machine. The numerical transfer function of a non-linear model differs from the linearized model. In the sense of parameter estimation, it means that parameters of the non-linear FE-model are different in comparison to the parameters of the linear FE-model. However, the machine in our consideration has quite linear saturation curve. The curve, provided by the manufacturer, is presented in Figure 12.

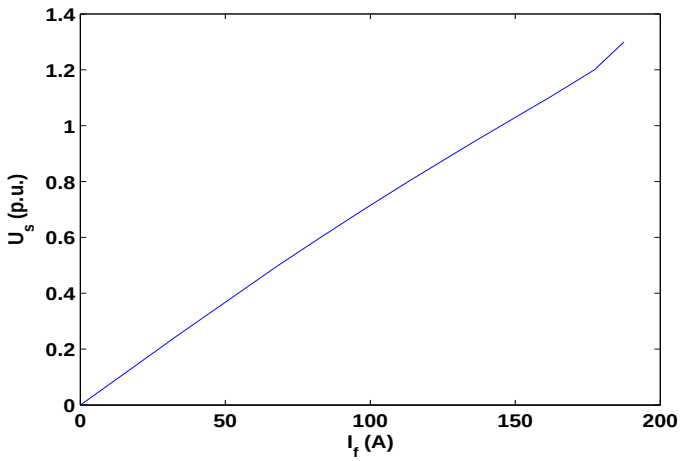

Figure 12 No-load voltage curve of the synchronous machine under investigation. The curve is almost straight, and therefore the saturation effect is small.

2.9 Cost function formulation

Least squares are used to formulate the cost function. The cost function is a measure of the goodness of the fit. The cost function evaluates deviation e_{i} between the simulated y_{s} value and the estimated value y_{se}. In order to take negative and positive deviations into account, the cost criterion is quadratic. In the case of least squares, the cost function has the following form

$$Q = \sum_i \left\| e_{\mathrm{i}} \right\|_2^2 \text{, where } e_i = \begin{bmatrix} Y_{\mathrm{s11i}} - Y_{\mathrm{se11i}} & Y_{\mathrm{s12i}} - Y_{\mathrm{se12i}} \\ Y_{\mathrm{s21i}} - Y_{\mathrm{se21i}} & Y_{\mathrm{s22i}} - Y_{\mathrm{se22i}} \end{bmatrix}$$

where the matrix norm is the Frobenius norm.

2.10 Differential Evolution algorithm

The Differential Evolution algorithm makes the minimization of the cost function. The algorithm is a global optimization method that is based on evolution strategies. Price et al. (2005) presented the theory and practice of the Differential Evolution algorithm in their book.

The basic schematic structure of the Differential Evolution algorithm is presented in Figure 13. First the population is initialized. Giving random values to every individual in population does it.

The selection chooses three vectors. Two of them form a difference vector, and the last vector from the three vectors will be mutated. The crossover population is comprised of the difference vector and the mutated vector. The crossover is performed between crossover population members. The evaluation selects the best performing individual among the best individual in the existing population and the offspring.

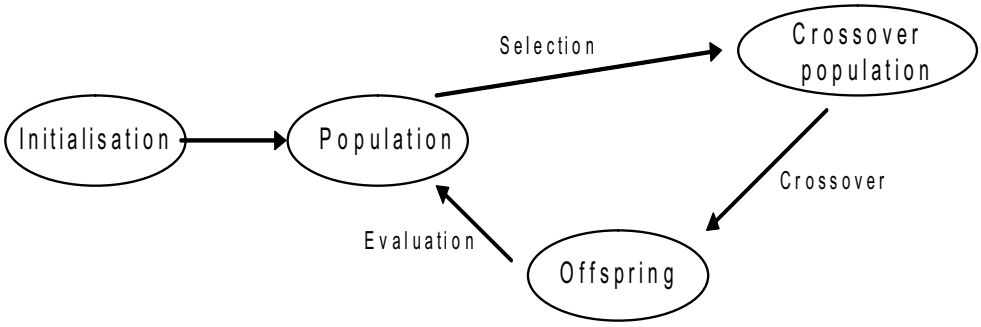

Figure 13 Basic working principle of the Differential Evolution algorithm.

2.11 Estimation process as a whole

The proposed estimation process for synchronous machines follows the process for induction machines presented by Repo et al. (2006a, 2006b & 2007). The basic idea is presented in the flow chart in Figure 14.

First in the estimation process, three simulations are made. One simulation is made without any impulse and two simulations with an impulse in both cases. The impulses are perpendicular to each other.

Second, we have to establish a formula for the deviation. It can be done numerically subtracting the simulation without an impulse from the one with an impulse.

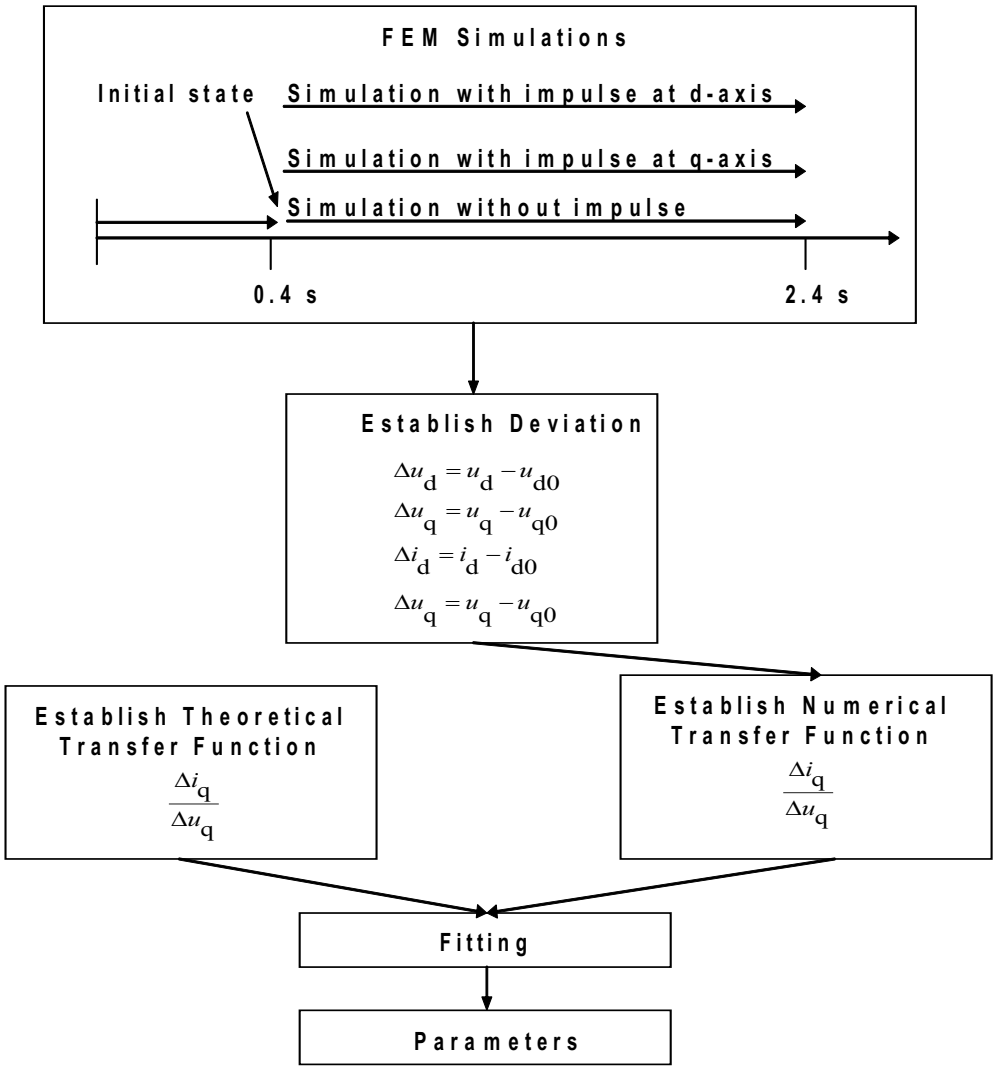

Figure 14 Flow chart of the parameter estimation procedure.

Third, a numerical and theoretical transfer function is formed. The numerical one is constructed using deviations, and the theoretical one is formed based on the two-axis model.

Fourth, the theoretical transfer function is fitted in the numerical transfer function data. The best fitting gives the parameters.

3 Results

3.1 Introduction

The machine under study is a 6-pole, Y-connected three-phase synchronous motor. The rated values are 12.5 MW, 3150V, 1-power factor, 50 Hz, and 1000 r/min.

In this study, the excitation is applied into stator voltage and the stator current response is recorded. The simulations are made with the FEM and for verification purposes with the circuit model. The FEM-simulations are made with a linear and non-linear machine model. In other words, we can consider the difference of results between the linear and non-linear machine models.

3.2 Operation points of the machine

The machine has been modeled using FEM at two operation points, close to the nominal operation point. The first one has linear material properties, Table 1. The second operation point considers non-linear properties of material, in Table 2. Due to change in material properties, the values of variables vary a little bit.

Table 1 First operating point. The FE-model is linear.

Variable	Value
Connection	star
EMF of the line	3150 V
Terminal voltage	3150 V
Terminal current	2352 A
Power factor	0.99 Cap.
Rotation angle	-151 El.deg.
Rotation speed	1000 rpm
Air-gap torque	120 kNm
Apparent power	12.8 MVA
Active power	12.7 MW
Reactive power	-1.5 MVAR
Shaft power	12.5 MW
Rotor voltage	65 V
Rotor current	390 A

Table 2 Second operating point. The FE-model is non-linear.

Variable	Value
Connection	star
EMF of the line	3150 V
Terminal voltage	3150 V
Terminal current	2432 A
Power factor	0.99 Ind
Rotation angle	-151 el. deg.
Rotation speed	1000 rpm
Air-gap torque	126 kNm
Apparent power	13.2 MVA
Active power	13.2 MW
Reactive power	259.8 kVAR
Shaft power	13.2 MW
Rotor voltage	65 V
Rotor current	389 A

3.3 Ran FEM simulations with FCSMEK

The finite element simulations are made with the FCSMEK finite element program. The code is developed in the Laboratory of Electromechanics at TKK.

The FEA process in FCSMEK has three stages. First we should create a finite element mesh, and it is generated based on information about dimensions and parameters of the electrical machine. Second, an initial state for time-stepping analysis is solved using a DC solution. Third, the time-stepping analysis is performed.

The FEM results are in the stator reference frame. Therefore, the variables are wanted to transform to the rotor reference frame. It can be done by the following transformations

$$u_{\mathrm{d}}^{\mathrm{k}} = \mathrm{Re}\left\{(u_{\mathrm{d}}+\mathrm{j}u_{\mathrm{q}})e^{\mathrm{j}\omega_{\mathrm{k}}\omega_{\mathrm{B}}t}e^{-\mathrm{j}\phi}\right\}$$

$$u_{\mathrm{q}}^{\mathrm{k}} = \mathrm{Im}\left\{(u_{\mathrm{d}}+\mathrm{j}u_{\mathrm{q}})e^{\mathrm{j}\omega_{\mathrm{k}}\omega_{\mathrm{B}}t}e^{-\mathrm{j}\phi}\right\}$$

$$i_{\mathrm{d}}^{\mathrm{k}} = \mathrm{Re}\left\{(i_{\mathrm{d}}+\mathrm{j}i_{\mathrm{q}})e^{\mathrm{j}\omega_{\mathrm{k}}\omega_{\mathrm{B}}t}e^{-\mathrm{j}\phi}\right\}$$

$$i_{\mathrm{q}}^{\mathrm{k}} = \mathrm{Im}\left\{(i_{\mathrm{d}}+\mathrm{j}i_{\mathrm{q}})e^{\mathrm{j}\omega_{\mathrm{k}}\omega_{\mathrm{B}}t}e^{-\mathrm{j}\phi}\right\}$$

k indicates the rotating frame, which rotates at speed ω_{k}. ω_{B} is the base frequency. ϕ denotes the angle between the d-axis in the stator and rotor reference frame after the transformation.

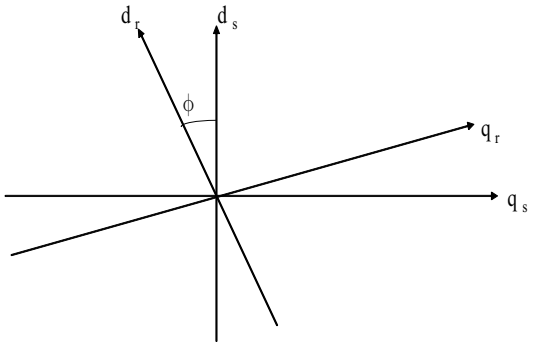

Figure 15 Angle between d-axis in stator and rotor's reference frame is defined to be ϕ. q_r, q_s and d_r, d_s depict the q-axis and d-axis in the rotor and stator reference frame, respectively.

After the transformation, it can be noticed that pulses, Δu_d and Δu_q, are on the d-axis and q-axis, Figure 17 and Figure 18, respectively.

The applied impulse in the stator voltage causes responses in stator currents. They are recorded and transformed to frequency domain. Also, the voltage impulse is transformed to frequency domain. The used voltage impulse is defined as follows

$$u_{imp} = a_{rel}\sqrt{2}u_{rms}\sin^2(2\pi ft) \tag{20}$$

u_{rms} is the average RMS-value of the line voltages. a_{rel} is the relative amplitude with respect to the voltage u_{rms}. t is 2.5 milliseconds and f is 200 Hz. The excited impulse has an amplitude size of 1% of the average RMS-value of the line voltages u_{rms}. According to Repo et al. (2007), this gives a non-zero frequency content at range from -750 to 800 Hz.

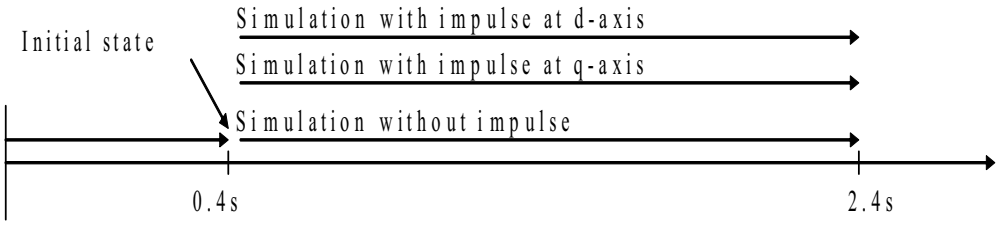

Figure 16 FEM simulation arrangements. The numerical impulse test consists of four FEM simulations. First, the initial state is computed and saved. Second, three different simulations are made from the initial state on, two simulations with perpendicular impulses and a simulation without any impulse.

The initial state is the state after 8000 time steps. One time step is 50 microseconds. There are 400 time steps in one period of line frequency. After the determination of the

initial state, FEM simulations are made using 40000 time steps. This gives a frequency resolution of 0.5 Hz. There are three different simulations in time interval from 0.4 seconds to 2.4 seconds. The first one is a simulation without an impulse. The second and the third are simulations with impulses at d- and q-axis.

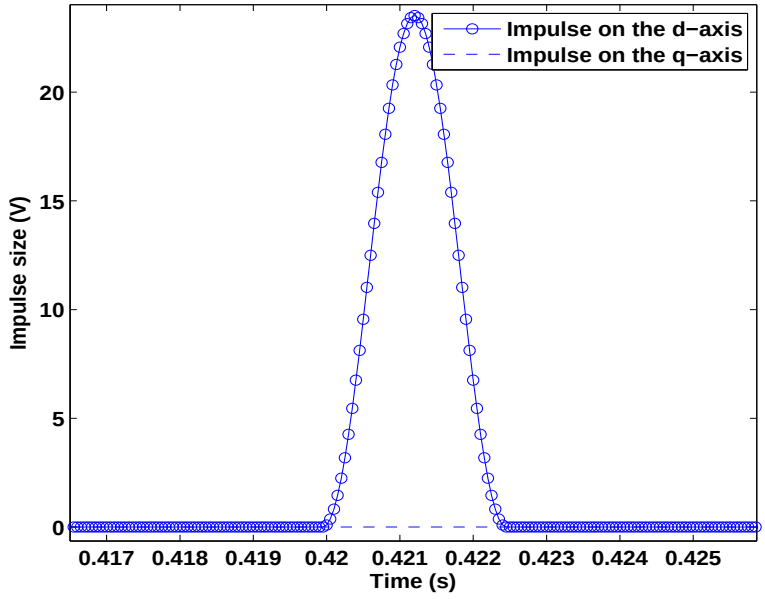

Figure 17 Direction of the impulses after the frame transformation on the d-axis.

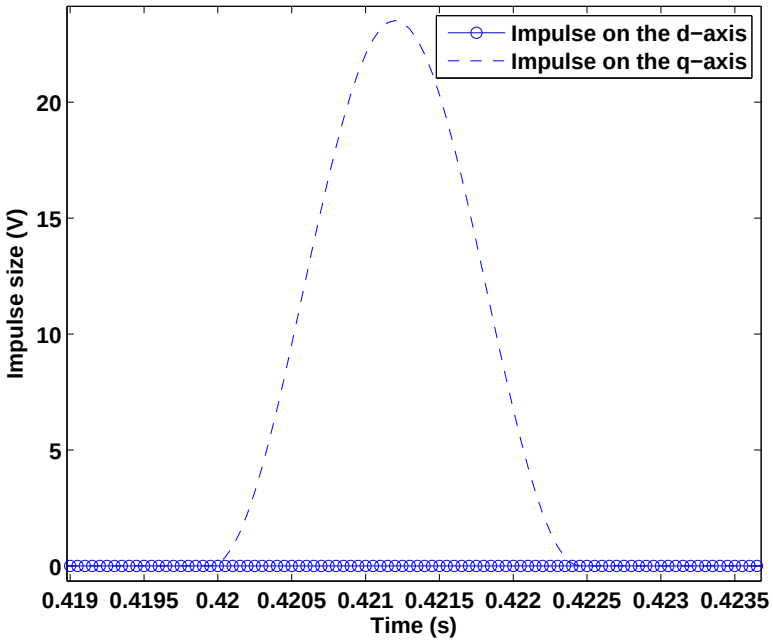

Figure 18 Direction of the impulses after the frame transformation on the q-axis.

This kind of approach is profitable; we can subtract the simulations with and without impulse from each other, and thus we can determine the deviation easily. The deviation in response can be specified in the same way.

$$\Delta u_{\mathrm{d}} = u_{\mathrm{d}} - u_{\mathrm{d0}}$$

$$\Delta u_{\mathrm{q}} = u_{\mathrm{q}} - u_{\mathrm{q0}}$$

$$\Delta i_{\mathrm{d}} = i_{\mathrm{d}} - i_{\mathrm{d0}}$$

$$\Delta u_{\mathrm{q}} = u_{\mathrm{q}} - u_{\mathrm{q0}}$$

u_{d} denotes simulation with impulse, and u_{d0} without impulse.

3.4 Frequency responses of FEM simulations

The frequency response analysis is made with FEM data. The obtained admittance frequency responses using linear material properties, in stator reference frame, are presented in Figures 19-22.

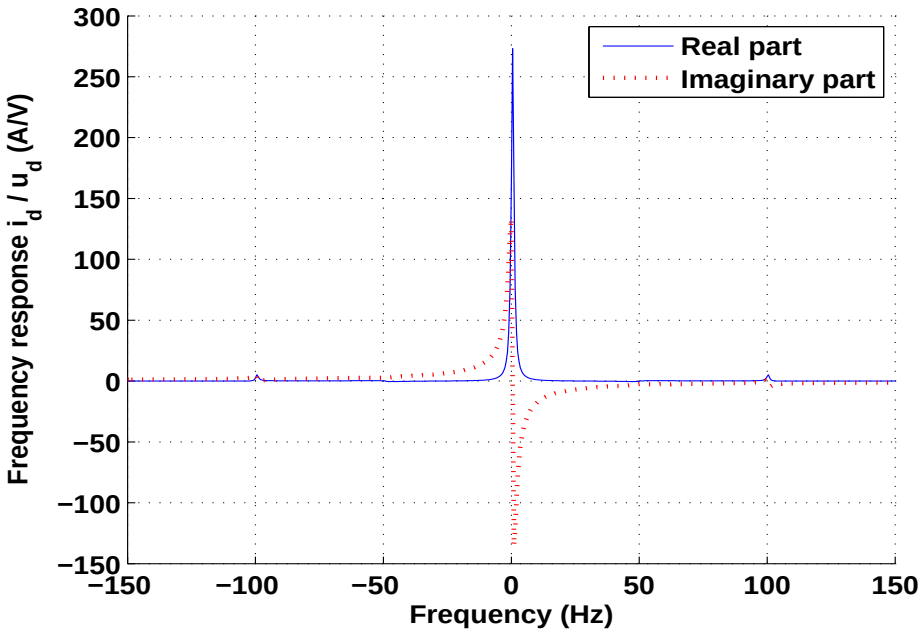

Figure 19 Frequency response of admittance $i_{\mathrm{d}} / u_{\mathrm{d}}$ using linearized FEM data. The real part is large at zero frequency. It means that even small DC voltage causes big DC-component in the current.

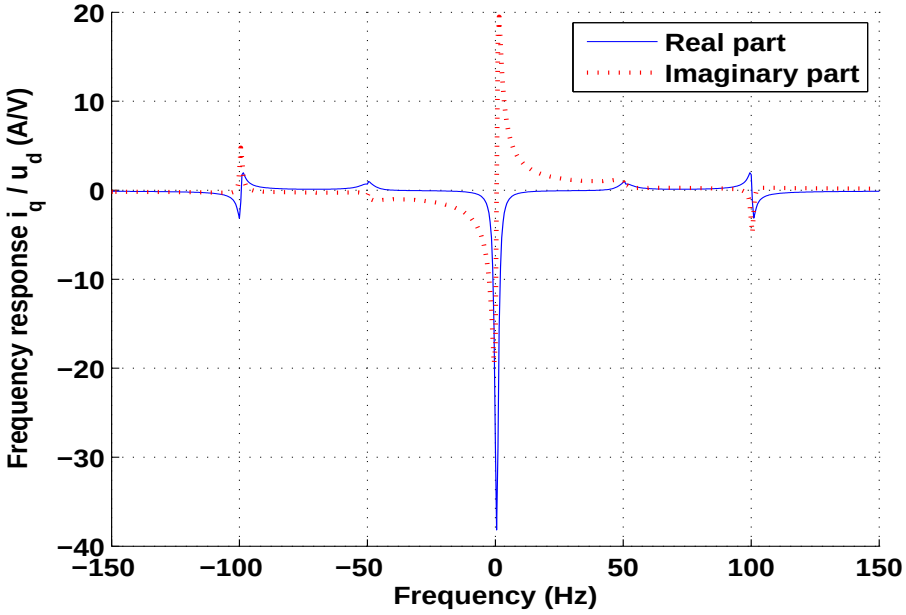

Figure 20 Frequency response of admittance i_q / u_d using linearized FEM data. The frequency response has a peak at zero frequency. However, it is a negative peak, and thus different compared to Figure 19.

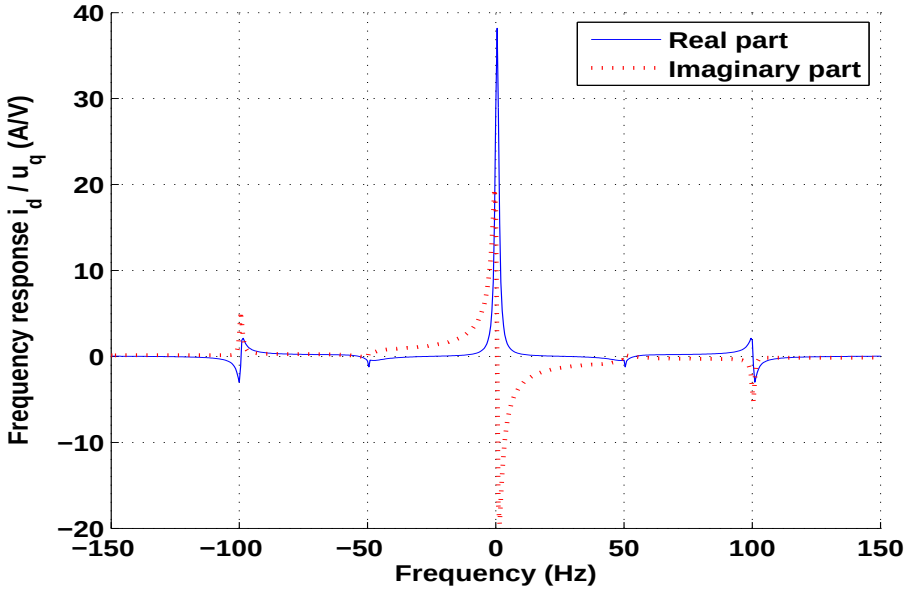

Figure 21 Frequency response of admittance i_d / u_q using linearized FEM data. The frequency response has low peaks at frequencies 50 Hz and 100 Hz.

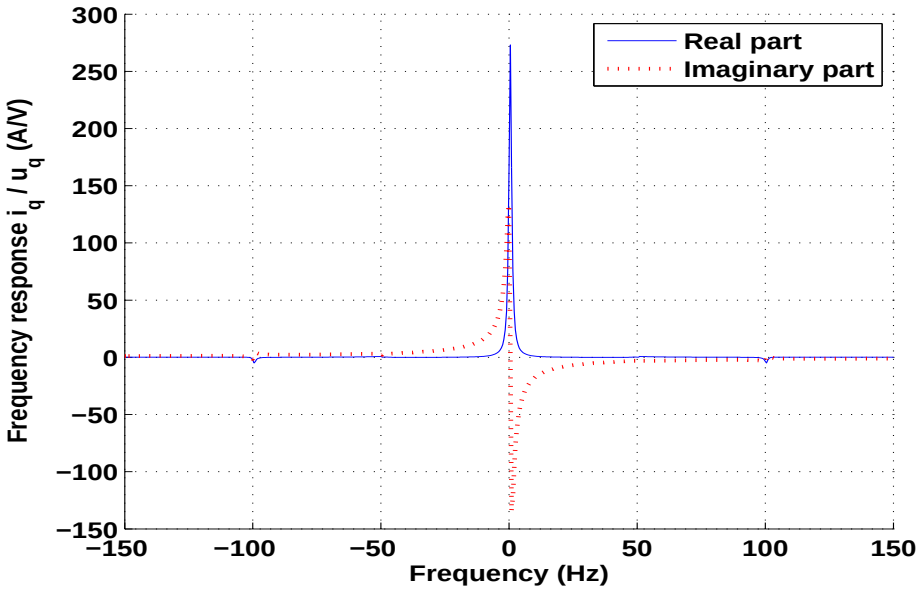

Figure 22 Frequency response of admittance using linearized FEM data. The frequency response is almost same as in Figure 16. Also this frequency response indicates big currents with small voltages.

From the frequency responses we can notice that the graphs have the same form but the amplitudes vary. In FEM simulated responses, there are low peaks at frequencies 50 and 100 Hz.

3.5 Effect of the impulse amplitude in the non-linear FE model

FEM simulations using the non-linear FE-model are performed and the effect of the impulse amplitude to the frequency response is studied. In order to perceive the applicability of the linear model, the effect of the impulse to the frequency response has to be small, and therefore the impulse has to be small enough. The impulse sizes 1%, 10% and 20% of the average RMS-value of the line voltages, u_{rms}, are used. The closer inspection is done about the rated frequency 50 Hz. The results are presented in Figures 23-26.

Figures 23-26 show that about at frequency 50 Hz, impulse sizes 10% and 20% of the u_{rms} make bigger errors in frequency response compared to the frequency response obtained by using impulse size of 1% the average RMS-value of the line voltages. It may be noticed that the estimated parameters using a 1% of amplitude differ from the parameters identified using bigger impulses. In some cases, the difference in frequency response can be even quite big. For instance in Figure 26, the imaginary part value using 1% impulse is about –0.5 A/V, and using 20% impulse the value is –0.7 A/V at frequency 51 Hz. The relative error is 0.2/0.5= 0.4 (40%).

However, at other frequencies than 50 Hz the error is very small. Table 3 presents the maximum error and the average error in the frequency interval –200 Hz to 200 Hz in the frequency response. The results show that, after all, the error in the frequency response due to the amplitude size is very small, on average, compared to the frequency response obtained by using impulse size of 1% of u_{rms}.

Table 3 Maximum and average error in the real and imaginary part with different impulse amplitudes compare to the 1- % of u_{rms} impulse size

	Amplitude of the impulse	Maximum error Real part (A/V)	Maximum error Imaginary part (A/V)	Average error Real part (A/V)	Average error Imaginary part (A/V)
$i_{\text{d}}/u_{\text{d}}$	10 %	0.2162	0.2443	0.0134	0.0109
	20 %	0.4540	0.5140	0.0288	0.0230
$i_{\text{q}}/u_{\text{d}}$	10 %	0.1158	0.0690	0.0040	0.0069
	20 %	0.2441	0.1445	0.0087	0.0145
$i_{\text{d}}/u_{\text{q}}$	10 %	0.0651	0.1171	0.0062	0.0035
	20 %	0.1366	0.2462	0.0133	0.0075
$i_{\text{q}}/u_{\text{q}}$	10 %	0.2387	0.2103	0.0111	0.0138
	20 %	0.5020	0.4425	0.0237	0.0292

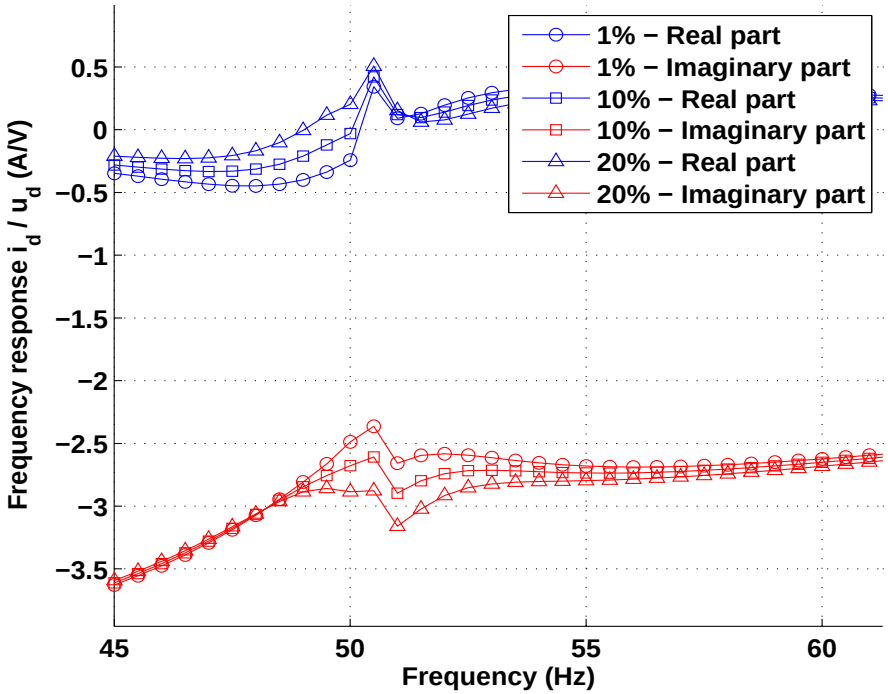

Figure 23 Frequency response comparison using different impulse amplitudes in the non-linear FE-model. The amplitude size of the impulse makes a slight difference about 50 Hz in the frequency response.

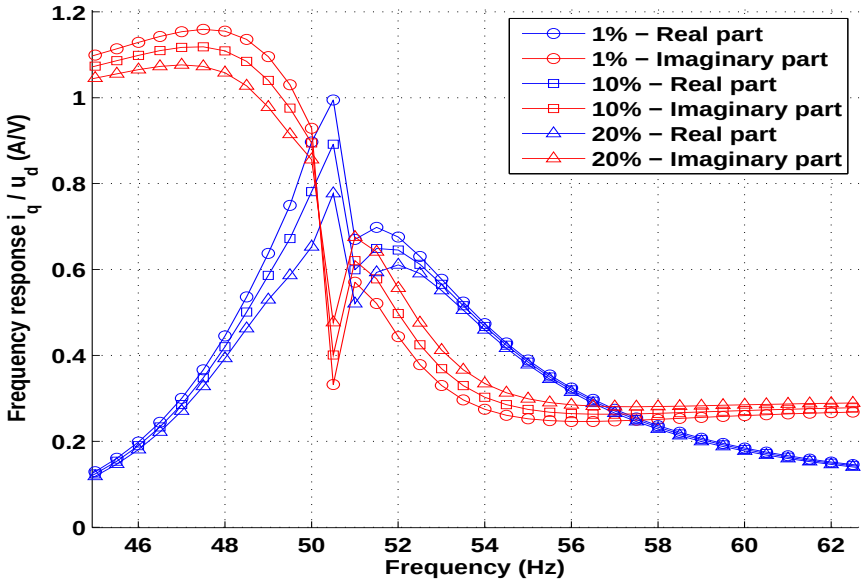

Figure 24 Frequency response comparison using different impulse amplitudes in the non-linear FE-model. The imaginary and real parts are closing each other in contrast to Figure 23, where they are getting further and further from each other about 50 Hz.

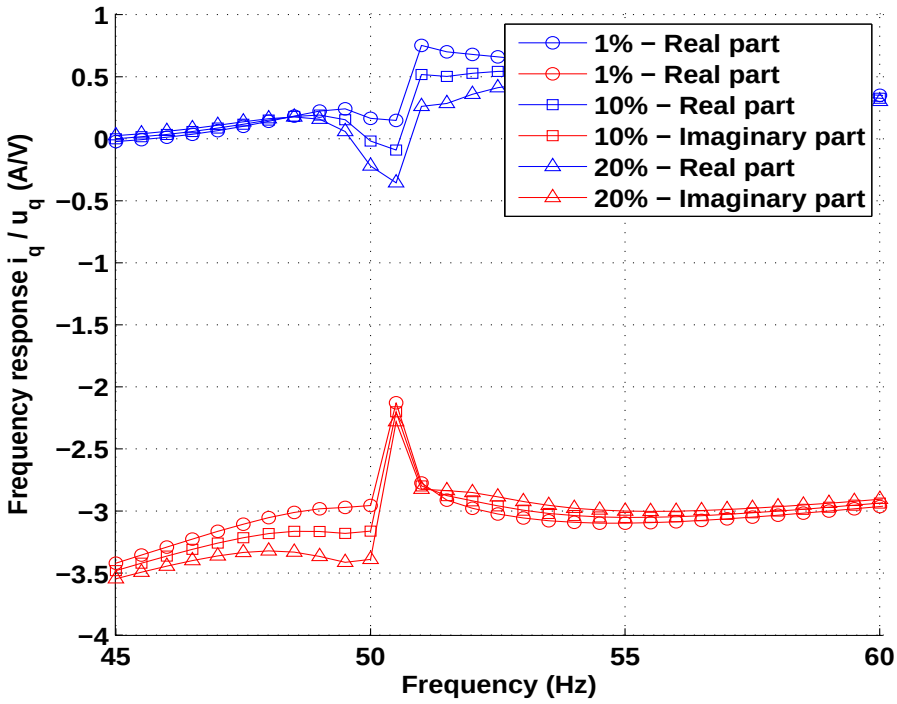

Figure 25 Frequency response comparison using different impulse amplitudes in the non-linear FE-model. The difference between different amplitude curves is quite big. The amplitude of the impulse does affect much to the transfer function between quadrature axis current and voltage about 50 Hz.

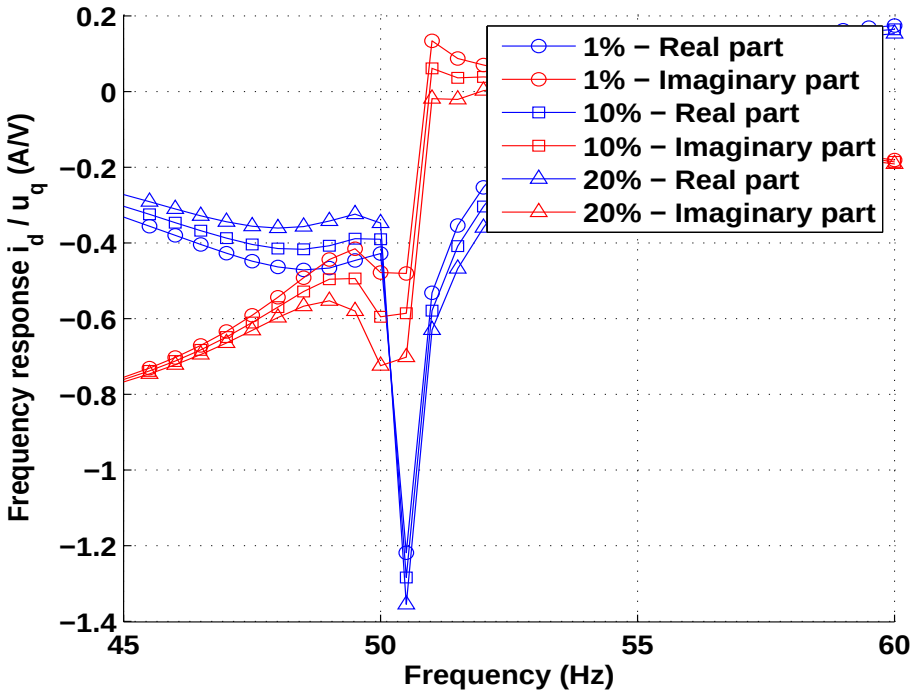

Figure 26 Frequency response comparison using different impulse sizes in the non-linear FE-model. The difference between different amplitude curves is quite small.

3.6 Curve fitting using Differential Evolution algorithm

In order to get the parameters of the machine, the theoretical transfer function is fitted in the numerical transfer function data points. The DE algorithm is used for the curve fitting. The crossover and weight factor values of the algorithm are 0.7 and 0.5. The search range is from 0 to 1. The population size is 1000, and the number of iterations is 7000. Resistances R_s and R_f are fixed to values given by the manufacturer, in order to decrease the number of parameter estimates.

3.6.1 Fitting results using the FEM data

The fitting is performed using two different FEM data. First, FEM data with linear material properties is used; second, data from FEM simulation with non-linear material properties is used.

In the simulation with a linear FE-model, all materials that have saturation are replaced by linear material. The relative permeability of the linear material is 1000. The success of the fit can also be viewed graphically. In the results, the absolute value and the angle of the matrix elements are presented. The diagonal elements are presented in Figure 27.

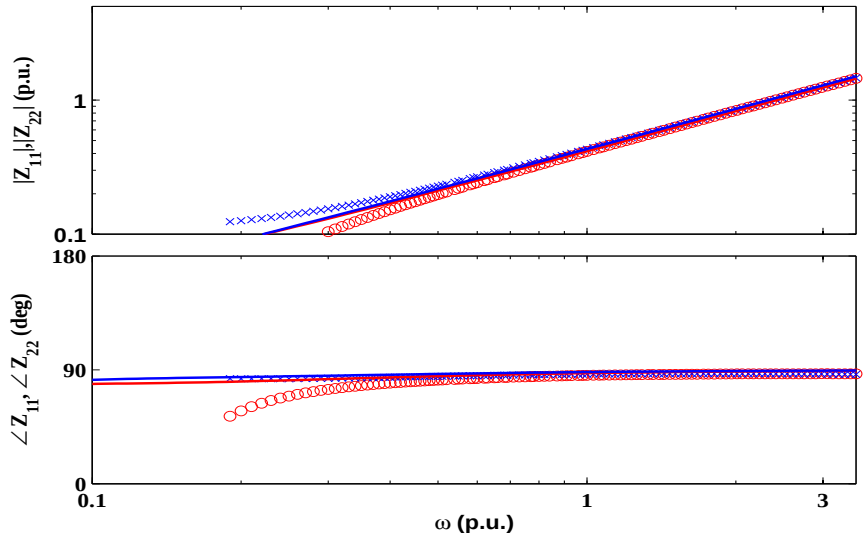

Figure 27 Fitting results of the diagonal elements to the FEM data. It can be noticed that the fitting succeeds well about frequency 1 (p. u.) and with larger frequencies.

The non-diagonal elements are in Figure 28, and it can be marked that they have a 180 degrees phase shift with respect to each other.

One may want to make a closer inspection about frequency 1 (p. u.). It is the range, which is sensible in normal operation. Figure 29 shows that the diagonal elements equal to each other. Absolute values of non-diagonal elements equal also to each other. The non-diagonal elements have a 180 degrees phase shift in angle.

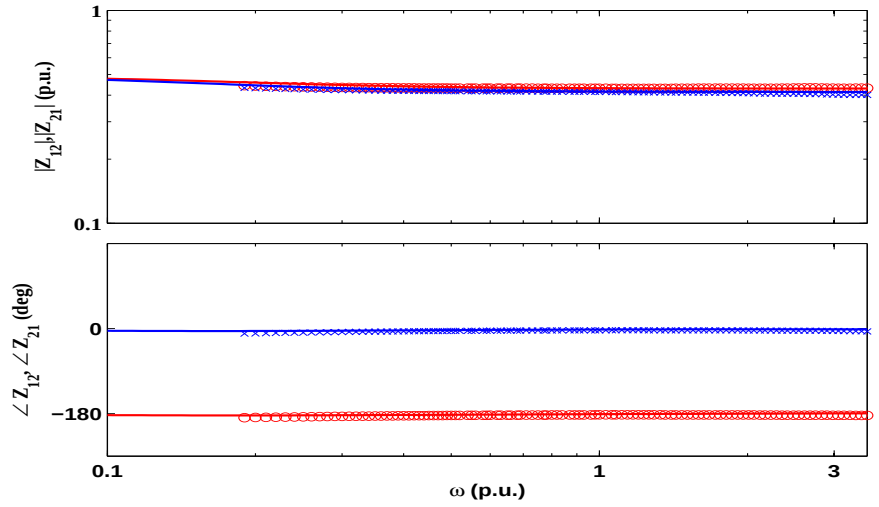

Figure 28 Fitting results of the non-diagonal elements to the FEM data. It can be marked that the fitting succeeds well over the whole frequency range.

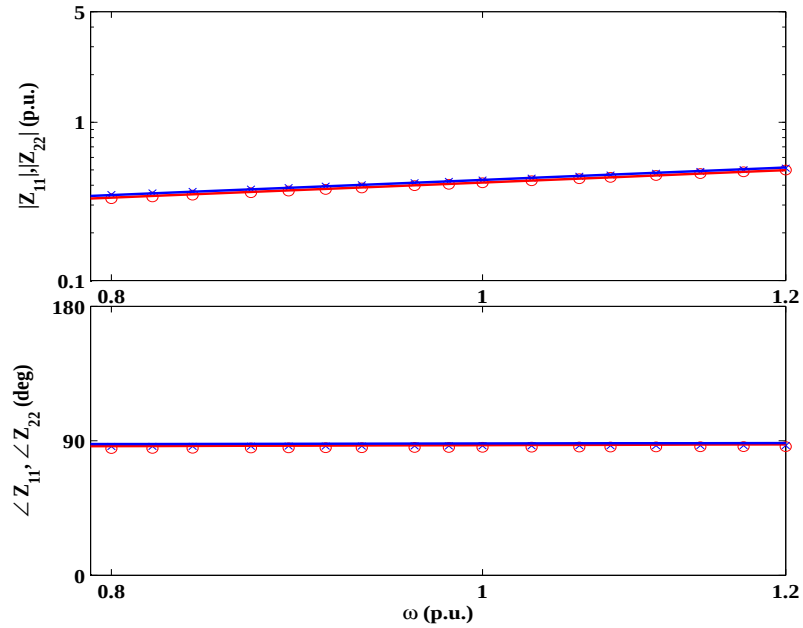

Figure 29 Fitting results of the diagonal elements, and a closer inspection about frequency 1. It can be noticed that the behavior about frequency 1 (p. u.) can be modeled well using the estimated parameters.

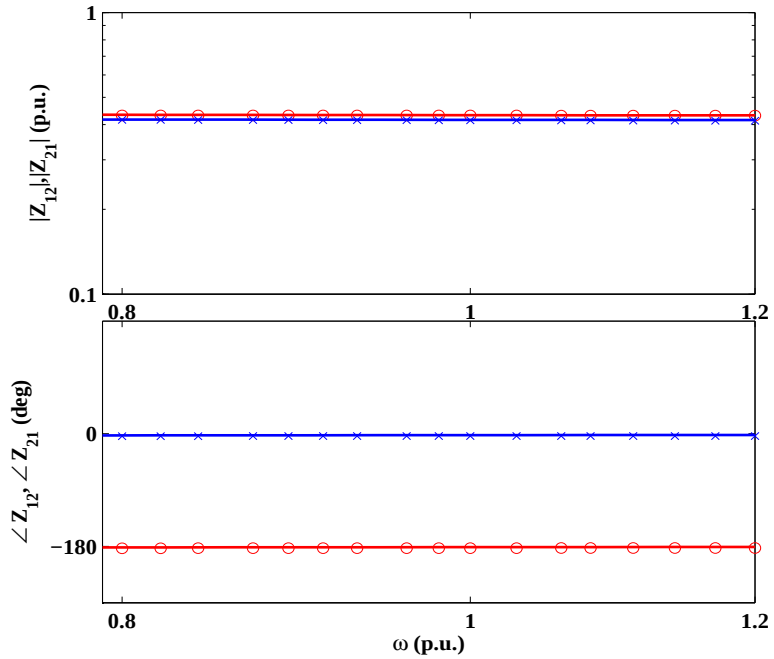

Figure 30 Fitting results of the non-diagonal elements, and a closer inspection about frequency 1 (p. u.). Like in case of diagonal elements, the non-diagonal elements agree very well with the FEM data.

The other simulation is made using non-linear material properties. The graphical presentation of the fitting results is in Figure 31 and in Figure 32. The diagonal elements are equal to each other as in the case of linear material.

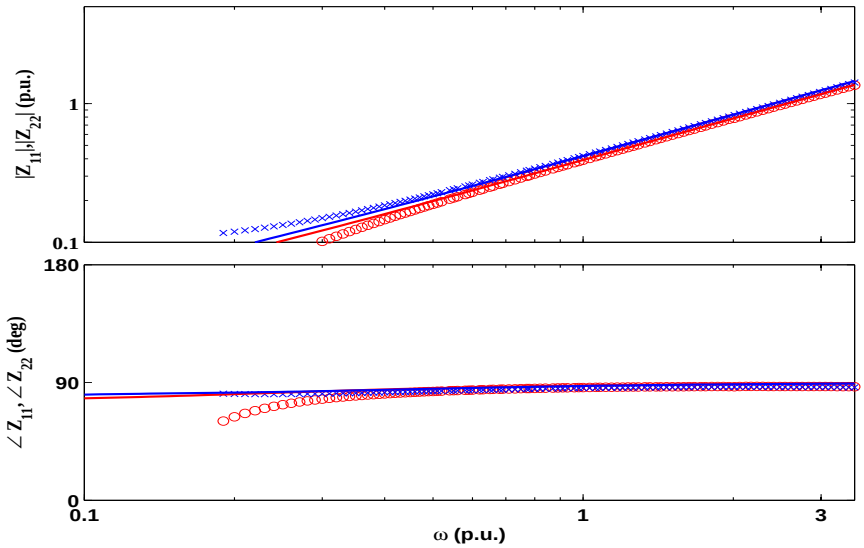

Figure 31 Fitting results of the diagonal elements with non-linear material properties. The fitting success follows well the fitting case with linear material properties in Figure 27.

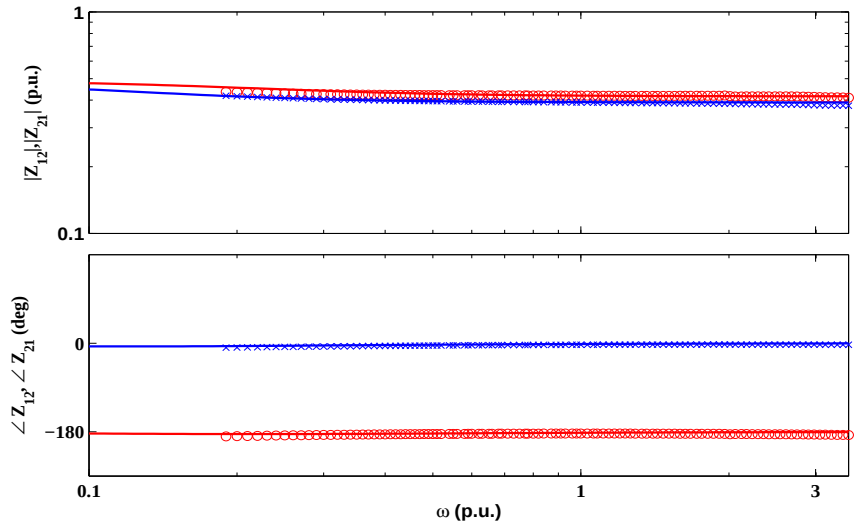

Figure 32 Fitting results of the non-diagonal elements with non-linear material properties. Like in the diagonal elements, the fitting success follows the case with linear material properties in Figure 28.

Properties of diagonal elements match also to characteristics of the diagonal elements with linear material. Non-diagonal elements have a 180 degrees phase shift. Also the

properties of non-diagonal elements match to properties of non-diagonal elements with linear material properties.

A closer inspection about frequency 1 (p. u.) tells that the fitting is a success about the normal operation point, and the obtained parameters describe the machine's behavior successfully. The fitting results of the diagonal elements around the frequency 1 are in Figure 33 and Figure 34.

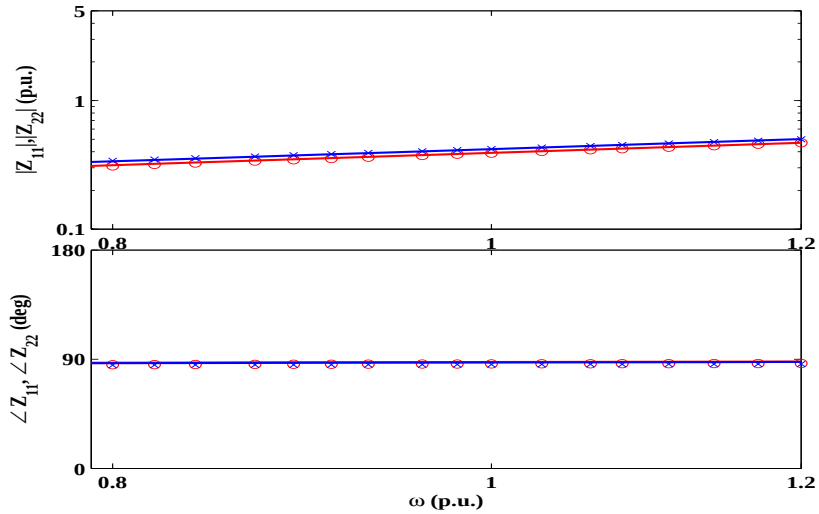

Figure 33 Fitting results of the diagonal elements, and a closer inspection about frequency 1 (p. u.). The fitting succeeds well in the neighborhood of the frequency 1 (p. u.) like in the case with linear material properties in Figure 29.

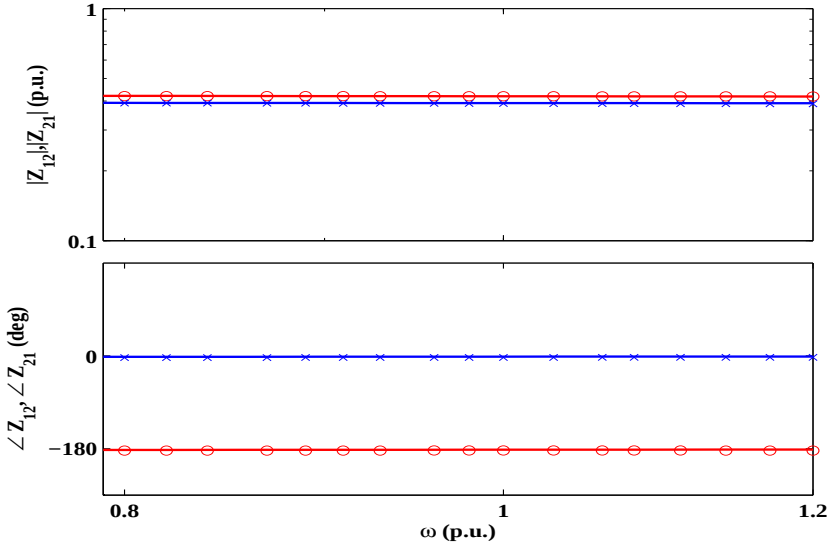

Figure 34 Fitting results of the non-diagonal elements, and a closer inspection about frequency 1 (p. u.). Like in the case of diagonal elements, the fitting success follows the case with linear material properties in Figure 30.

3.7 Circuit model simulations

For verification purposes, simulations are also made with the circuit model in the Simulink environment. The synchronous machine model is constructed. The model is based on the two axis model and the voltage equations are in the synchronous reference frame. The torque equation is not taken into consideration. Three different models are used. The models are same but the inputs differ. The first model simulates steady-state operation, and there is no impulse as input. The second model simulates operation under an impulse in the d-axis as input, and the third model, which applies an impulse in the q-axis as input. The parameters for the circuit model are the estimated parameters with linear material properties. The comparison between frequency responses obtained by using the circuit model and the FE model makes the verification of the used methods.

In the circuit model, the impulse can be addressed either to d- or q-axis. It is possible due to transformation from the 3- to 2-phase system. It is done using Park's theorem. The three-phase variables can be expressed in the two-phase system using the following matrix

$$\begin{bmatrix} i_\alpha \\ i_\beta \\ i_0 \end{bmatrix} = \frac{2}{3} \begin{bmatrix} 1 & -\frac{1}{2} & -\frac{1}{2} \\ 0 & \frac{\sqrt{3}}{2} & -\frac{\sqrt{3}}{2} \\ \frac{1}{2} & \frac{1}{2} & \frac{1}{2} \end{bmatrix} \begin{bmatrix} i_a \\ i_b \\ i_c \end{bmatrix} \tag{21}$$

The inverse transformation, the transformation from the two-phase to three-phase system, may be presented as below

$$\begin{bmatrix} i_a \\ i_b \\ i_c \end{bmatrix} = \frac{2}{3} \begin{bmatrix} 1 & 0 & 1 \\ -\frac{1}{2} & \frac{\sqrt{3}}{2} & 1 \\ -\frac{1}{2} & -\frac{\sqrt{3}}{2} & 1 \end{bmatrix} \begin{bmatrix} i_\alpha \\ i_\beta \\ i_0 \end{bmatrix} \tag{22}$$

The realization of the circuit model with Simulink blocks is presented in Appendix 1.

3.8 Frequency responses of the circuit model

The obtained admittance frequency responses, in stator reference frame, are presented in Figures 35-38.

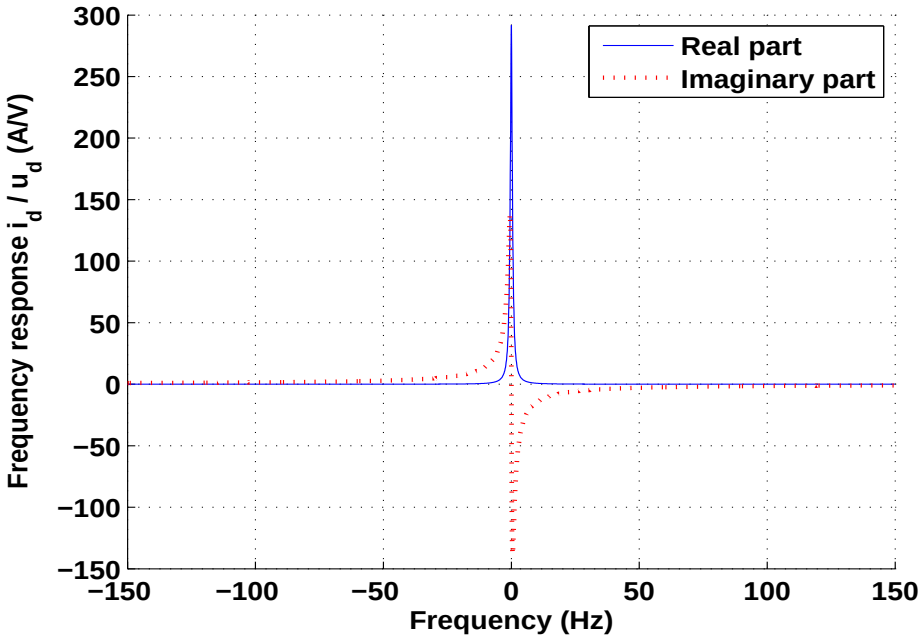

Figure 35 Frequency response of admittance i_d / u_d in Simulink. The frequency response matches well to the frequency response obtained by using FEM data, Figure 19.

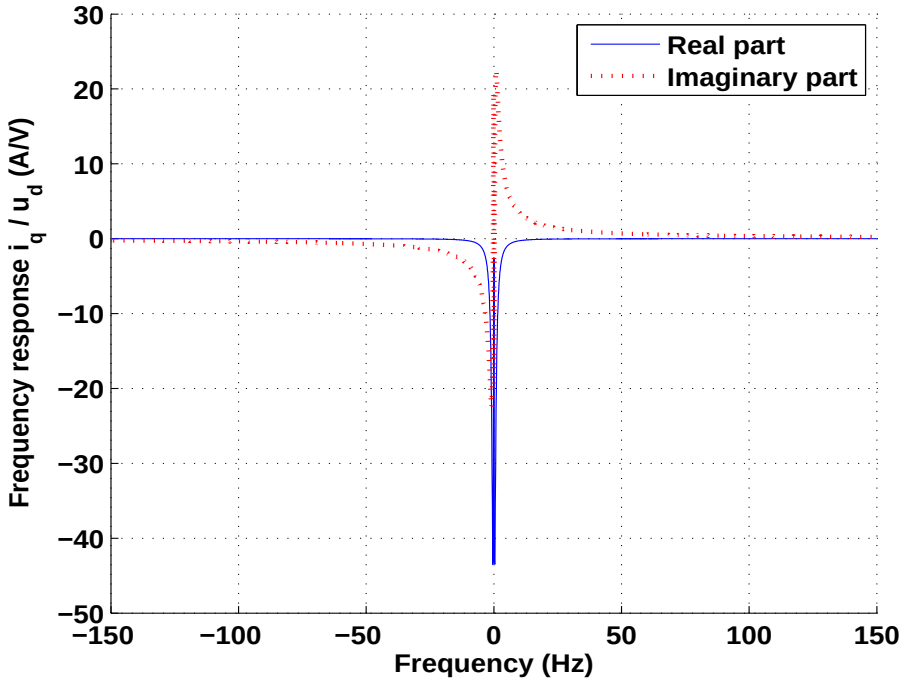

Figure 36 Frequency response of admittance i_q / u_d in Simulink. The response matches to the frequency response obtained by using FEM data, Figure 20. At frequencies 50 Hz and 100 Hz the FEM frequency response has low peaks that are not depicted by the circuit model.

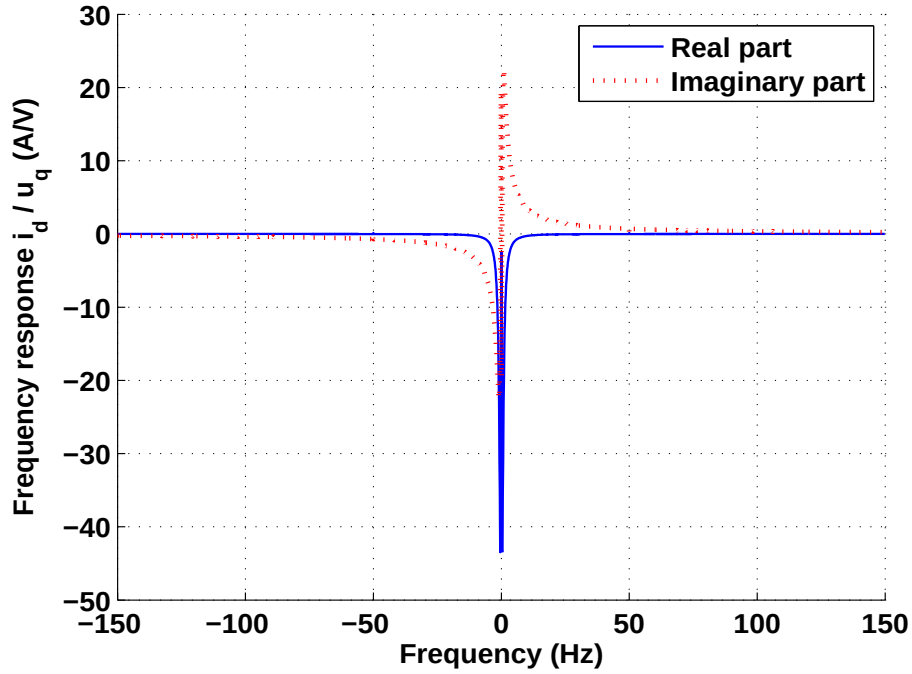

Figure 37 Frequency response of admittance $i_{\mathrm{d}} / u_{\mathrm{q}}$ in Simulink. The frequency response follows the form of the frequency response obtained by using FEM, Figure 21. However, the low peaks at 50 Hz and 100 Hz do not appear in the circuit model.

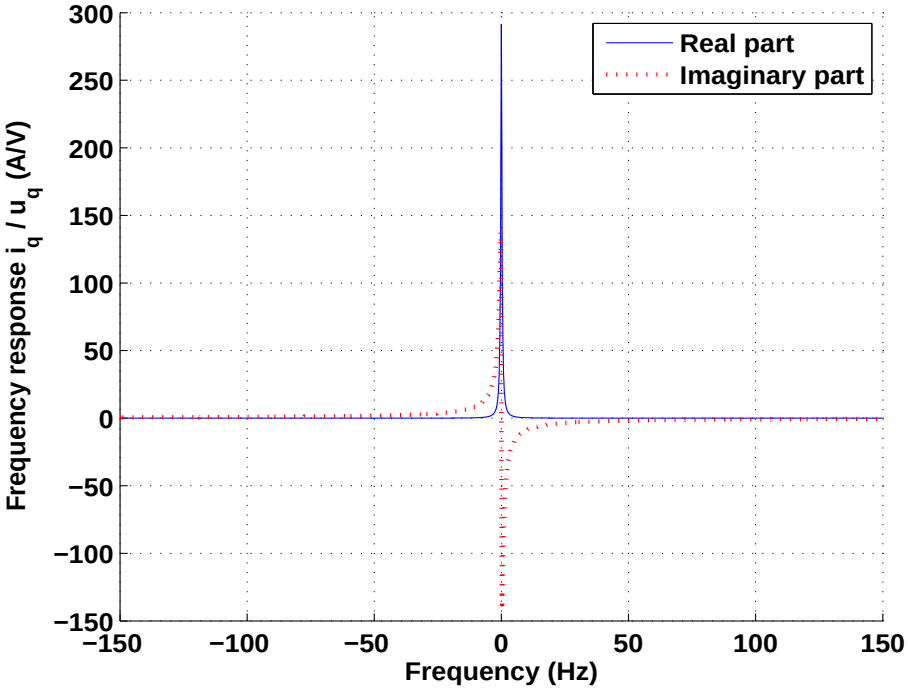

Figure 38 Frequency response of admittance $i_{\mathrm{q}} / u_{\mathrm{q}}$ using Simulink. The frequency response matches well to the frequency response obtained by using the FEM data, Figure 22.

3.9 Obtained parameters

Figures 27-34 show that the fitting succeeded well about the base frequency and at large frequencies. At small frequencies (0 - 1 p. u.) of diagonal elements, the fit is not good. The same behavior can be seen in the nonlinear and linear case.

The saturation does not make a big difference in the fit nor frequency response. It is expected because the no-load voltage curve is almost straight. The results with nonlinear material properties are almost the same as the results with linear material properties.

The obtained parameters are referred to stator, and they are in per units. The values of the stator resistance and magnetizing resistance are fixed to the values given by the manufacturer, and thus the number of cost function minima is decreased. The parameters of the two-axis model are listed in Table 4. The parameters given by the manufacturer are in Appendix 2. According to Verbeeck, J. et al. (1999), there is not a unique set of parameters, and therefore both parameter sets may be valid.

It can be seen that the parameter values, obtained using the linear FE-model or non-linear FE-model, are close to each other. It is also expected due to the fact that the saturation curve in Figure 12 is almost linear.

The parameters describe well the behavior of a synchronous machine when the two-axis model is used. Simulink simulations gave same results as the FEM simulations. The similarity is verifying the methods that are used, and the applicability of the numerical impulse method in parameter estimation for a synchronous machine.

Table 4 Obtained parameters. The value of the stator and excitation winding resistance were fixed to the values before the curve fitting process. Parameters with the mark * were not estimated.

Description	Symbol	Value (p. u.) Linear FE-model	Value (p. u.) Non-linear FE-model
Stator resistance	R_s *	0.0047	0.0047
Stator direct-axis inductance	L_{sd}	0.6547	0.8514
Stator quadrature-axis inductance	L_{sq}	0.4855	0.5812
Direct axis magnetizing inductance	L_{md}	0.3369	0.4665
Quadrature axis magnetizing inductance	L_{mq}	0.2324	0.3896
Excitation winding inductance	L_f	0.9914	0.9986

Excitation winding resistance	R_f *	0.0009	0.0009
D-axis damper winding inductance	L_D	0.8937	0.8973
D-axis damper winding resistance	R_D	0.1001	0.0403
Q-axis damper winding inductance	L_Q	0.9791	0.9289
Q-axis damper winding resistance	R_Q	0.2075	0.0838

3.10 Parameters at different operation points

The parameters were also estimated at different operation points. The points were about 0.5MW, 6MW and 12.5 MW, and the results are presented in Figure 39-42. It can be noted that the change of some parameters is remarkable between two different operation points. It may be that they substitute each other partly at different operation points during the optimization process, and therefore they do not present physical variation of the parameters. However, the fitting succeeded equally well at every point, and therefore the parameters present well the behavior of the machine at a certain point.

Also, the DE algorithm works well. The algorithm has been tested by estimating the parameters three times in row at one operation point. The algorithm converged to the same minimum every round. However, according to Verbeeck, J. et al. (1999), there is not a unique set of parameters, and therefore an other global minimum may also be reached. A drawback of the algorithm is a big population size of 1000 members, and the number of iteration rounds. In this case the number of iterations was 7000 rounds. Another drawback is the high time consumption of DE. However, the DE is adequate for the optimization process if the two disadvantages above are considered small.

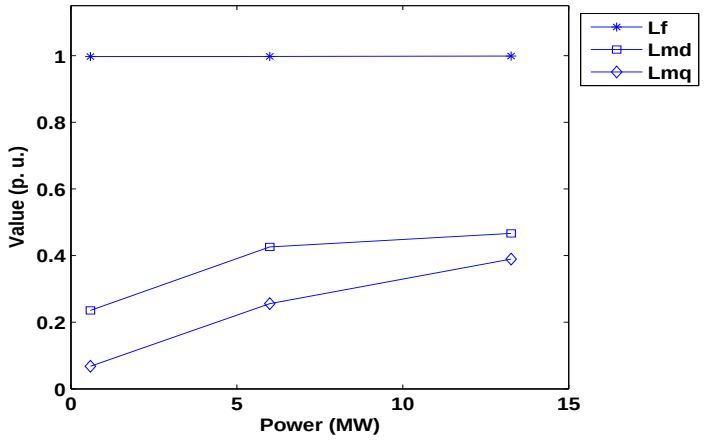

Figure 39 L_{md} , L_{mq} and L_f at different operation points. The inductance of the excitation winding is constant and magnetizing inductances increase over the power interval.

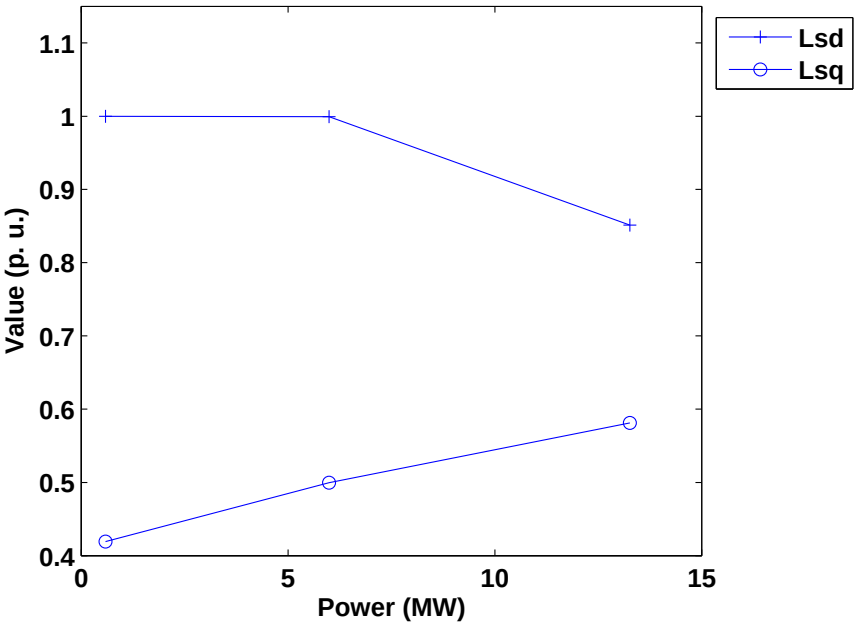

Figure 40 Stator leakage inductances L_{sd} and L_{sq} over the power interval.

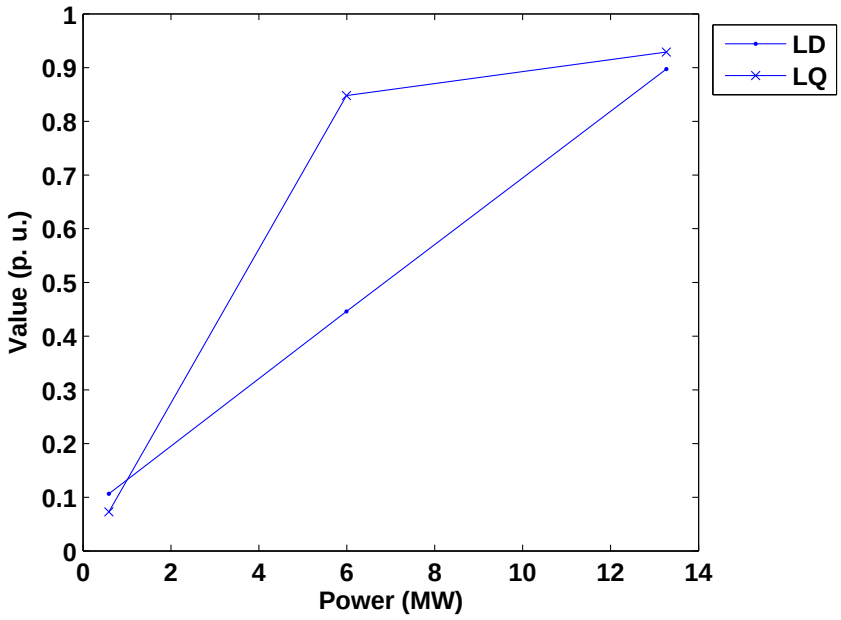

Figure 41 Damper winding inductances L_D and L_Q over the power interval.

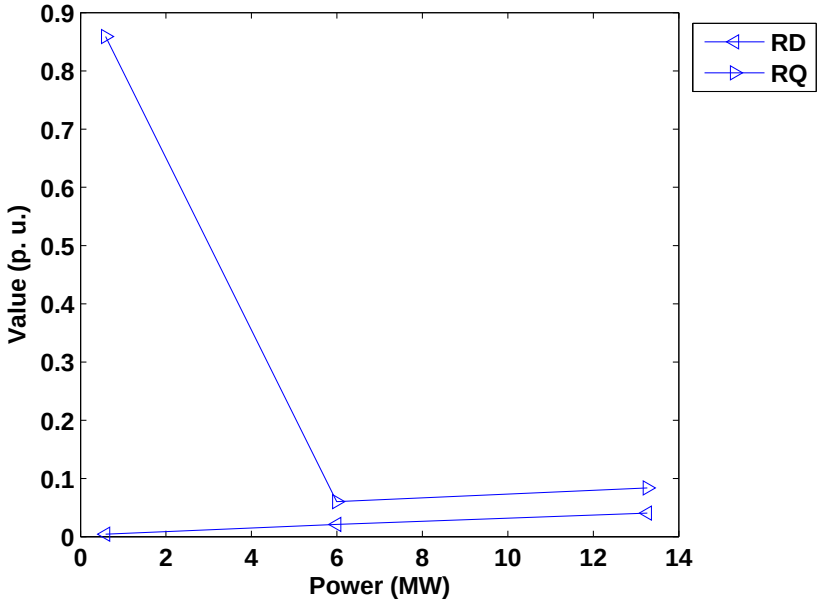

Figure 42 Damper winding resistances R_{D} and R_{Q} over the power interval.

4 Discussion

The two axis model parameters of a synchronous machine have been estimated using the numerical impulse method. Unlike the standstill frequency response test, the proposed method is describing the behavior of the machine at other operation points as well. The parameters are extracted from the data using an evolution algorithm. The obtained parameters have been verified using circuit simulations in the Simulink-environment.

Although, the standard two axis model and the estimated parameters describe the behavior of the machine well, higher order models may be more interesting. An accurate prediction of machine's behavior is desirable. Also, the model that takes the mutual inductance between excitation and damper windings into account may be of interest in many cases. Research of the applicability of the impulse response method in the cases above may be reasonable in the future.

The number of time-stepping finite element simulations might be possible to decrease compare to the arrangement presented in Figure 16. If the behavior of the machine is considered linear about an operation point, only one time-stepping finite element simulation might be needed. Based on the results, the linear behavior of the machine is a reasonable approximation about an operation point. Thus, the time consumption of the simulation stage could be decreased.

The minimization of the cost function has been made using an evolution algorithm called Differential Evolution. The algorithm suits well for the minimization. The algorithm did catch the same minimum every time. The size of the population needs to be high, as well as, the number of iteration rounds. However, according to Verbeeck, J. et al. (1999), there are many global minima in the case when there are more than one damper winding on the axis. Therefore the algorithm may converge also to another global minimum, and the same values are not obtained.

The minimization can possibly be made using the Newton iteration or another conventional optimization method also. It may be that, for example, the Newton iteration needs good initial values so that it converges, but in the case of convergence, the Newton iteration is fast. In the neighborhood of the solution, the convergence of the Newton iteration is quadratic. Optimization using an evolution algorithm is time-consuming, and therefore, the possibility to apply Newton iteration, for instance, in context of the numerical impulse method is interesting.

Good initial values for the iteration may be achieved using the properties of the frequency response. There is a publication written by Henschel et al. (1999), which covers an idea obtaining the values of the parameters directly from the frequency response. The idea may be interesting, and the suitability with the numerical impulse method may be investigated in the future.

Saturation does not affect much in the investigated machine but a model for saturation may be of interest in cases where saturation effects are noticeable. The model should be built and the applicability of the model should be tested in context of the numerical impulse method.

The parameters have been estimated at different operation points and it can be noticed that the variation in parameters may not be the physical variation of the parameters. They may substitute each other partly at different points. However, they describe well the behavior of the machine at operation points. In the future, it may be reasonable to try to change the optimization process so that the variations of the parameters describe the physical variations of the parameters. Also, the fit at low frequencies is not good. This issue is also of interest in the future.

Measurements are needed in order to verify the obtained parameters. To obtain the frequency responses under study, the harmonic excitation experiments may be needed. However, the frequency responses obtained using the Simulink circuit model with estimated parameters match well with FEM simulations.

The studied machine is a salient pole synchronous machine with an excitation winding. However, in the future, permanent magnet synchronous machines are getting more and more common. Therefore, the applicability of the numerical impulse method is of interest in context of permanent magnet synchronous machines.

5 Conclusion

The suitability of the numerical impulse method for the synchronous machine parameter estimation has been studied. The two-axis model parameters have been estimated using FEM data, and the results are reasonable. The parameters are valid about the operation point selected. The parameters have been estimated using linear and nonlinear material FE-models. The estimated parameters are verified using circuit simulations in the Simulink environment. The results obtained from the circuit and FEM simulations match well with each other.

Linearized equations may be used for describing the behavior about an operation point. A linearization method for the two-axis model equations taking advantage of the Taylor's expansion is presented. From the linearized equations a transfer function between the current and voltage will be formulated. A formulation exploiting results in control theory has been presented. Lastly, the transfer function is fitted into the numerical transfer function produced by FEM simulations, and thus the parameters can be achieved.

The fitting is made using a Differential Evolution algorithm. It has been noticed that it is easy to use and an effective tool for the fitting process. The algorithm does converge to the minimum round after round, but the size of population members is high, as well as, the number of iteration rounds. In case of more than one damper winding, there are n factorial (n!) global minima. A drawback in the Differential Evolution algorithm is the time consumption.

The obtained values of the parameters, using the linear and non-linear FE-model are quite close to each other. The result is expected because the magnetizing curve is almost linear. It also seems that the parameters describe well the desired input/output behavior based on the experiments made using the circuit model in the Simulink environment.

An MIMO-system model for a synchronous machine is presented. In that representation, the outputs and inputs are the d- and q-axis currents and voltages, and the transfer function is a 2x2 admittance or impedance matrix. In the optimizing process, the size of the matrix is measured by the Frobenius norm.

The permitted impulse size in the circuit model has been studied using Lyapunov stability analysis. It can be interpreted that there is only one steady state, and the system is stable regardless of the impulse size.

The effect of the amplitude of the impulse in the FEM-simulations using the nonlinear material FE-model has been studied using three different impulse amplitudes, 1%, 10% and 20% of the average RMS-value of the line voltages. It can be noticed that the difference in frequency responses is very small, and the effect of the impulse amplitude is small with the studied amplitudes. Therefore the linearization about an operation point is reasonable.

The numerical impulse method is suitable for the parameter estimation of synchronous machines. The great advantage of the impulse method is that the obtained parameters describe the real operation point of the machine. Also the saturation is considered. Additionally, the proposed method is not stressful on experimental measurements for the machine because high current peaks can be avoided, unlike in the sudden short circuit test.

6 References

Bastos, J. P. A. & Sadowski N. 2003, Electromagnetic Modelin by Finite Element Methods, Marcel Dekker, Inc., New York

Bortoni, E. C. & Jardini, J. A. 2004, A Standstill Frequency Response Method for Large Salient Pole Synchronous Machines, IEEE Transactions on Energy Conversion, Vol. 19, No. 4, December 2004, pp. 687-691

Burakov, A. & Arkkio, A. 2006, Low-order parametric force model for a salient-pole synchronous machine with eccentric rotor, Electrical Engineering 89: 127-136

Electric Machinery Committee of the IEEE Power Engineering Society 1995, IEEE Guide: Test Procedures for Synchronous Machines

Glad, T. & Ljung, L. 2000, Control Theory: Multivariable and Nonlinear Methods, Taylor & Francis, Great Britain

Henschel, S. & Dommel, H. W. 1999, Noniterative Synchronous Machine Parameter Identification from Frequency Response Tests, IEEE Transactions on Power Systems, Vol. 14, No. 2, May 1999, pp. 553-560

Holopainen, T. 2004, Electromechanical interaction in rotordynamics of cage induction motors, VTT Publications 543. Online: http://lib.tkk.fi/Diss/2004/isbn9513864057/

Keyhani, A. & Tsai, H. 1994, Identification of High-Order Synchronous Generator Models from SSFR Test Data, IEEE Transactions on Energy Conversion, Vol. 9, No. 3, September 1994, pp. 593-603

Krause, P. C., Wasynczuk, O. & Sudhoff, S. D. 2002, Analysis of Electric Machinery and Drive Systems, Wiley-Interscience, USA

Luomi, J. 1998, Transient Phenomena in Electrical Machines, lecture notes at Chalmers University of Technology, Göteborg

Luomi, J., Niiranen, J. & Niemenmaa, A. 2005, Sähkömekaniikka ja sähkökäytöt osa 2 (in Finnish), Helsinki University of Technology, Espoo

Müller, G. 1985, Elektrische Maschinen: Betriebsverhalten rotierender elektrischer Maschinen, VEB Verlag Technik Berlin

Price, K. V., Storn R. M. & Lampinen J. A. 2005, Differential Evolution A Practical Approach to Global Optimization, Springer, Heidelberg

Repo, A. -K. & Arkkio, A. 2006a, Parameter estimation of induction machines using the numerical impulse method, SPEEDAM 2006 23-26 May, Taormina Italy, International Symposium on Power Electronics, Electrical Drives, Automation and Motion, 2006, pp. 943-948

Repo, A. -K. & Arkkio, A. 2006b, Numerical impulse response test to estimate circuit-model parameters for induction machines, IEE Proceedings-Electrical Power Applications, Vol. 153, No.6, November 2006, pp. 883-890

Repo, A.-K. & Arkkio, A. 2007, Numerical impulse response test to identify parametric models for closed-slot deep-bar induction motors, IET Electrical Power Applications, Vol. 1, No. 3, May 2007, pp. 307-315

Struble, R. A. 1962, Nonlinear Differential Equations, McGraw-Hill Book Company

Tenhunen, A. 2003, Electeromagnetic forces acting between the stator and eccentric cage rotor, Doctoral Thesis, Helsinki University of Technology, Laboratory of Electromechanics, Report 69, Espoo 2003. Online: http://lib.tkk.fi/Diss/2003/isbn9512266830/

Verbeeck, J., Pintelon, R. & Guillaume, P. 1999, Determination of Synchronous Machine Parameters Using Network Synthesis Techniques, IEEE Transactions on Energy Conversion, Vol. 14, No. 3, September 1999, pp. 310-314

Wamkeue, R., Kamwa, I. & Chacha M. 2003, Line-to-Line Short-Circuit-Based Finite-Element Performance and Parameter Predictions of Large Hydrogenerators, IEEE Transactions on Energy Conversion, Vol. 18, No. 3, September 2003, pp. 370-378

7 Appendixes

Appendix 1: Simulink model

The Simulink model works in rotor reference frame and all variables are referred to stator. The simulation model is presented in Figure A1. The model in Figure A1 is a situation where the impulse is applied to the d-axis. The impulse to q-axis can be made changing the sum block to q-axis and connecting the impulse block to the sum block. In the steady-state simulation, the 'Impulse1'-block is unconnected.

The transformation from the 3 to 2 phase system (block 'abc->dq rotor') is presented in Figure A2. The same block makes also the transformation to the rotor reference frame. The realization of the 'Impulse1'-block is in Figure A3. It generates the impulse. The synchronous machine equations, without mechanical equation, are realized in Figure A4. It follows the conventional two axis model. The RungeKutta method makes the integration, and the fixed step size is chosen to be 0.0005 seconds.

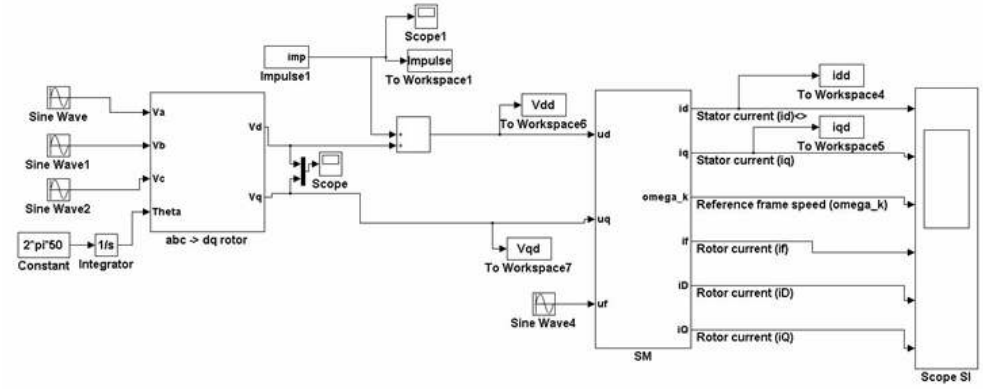

Figure A1 Schematic diagram about simulation environment.

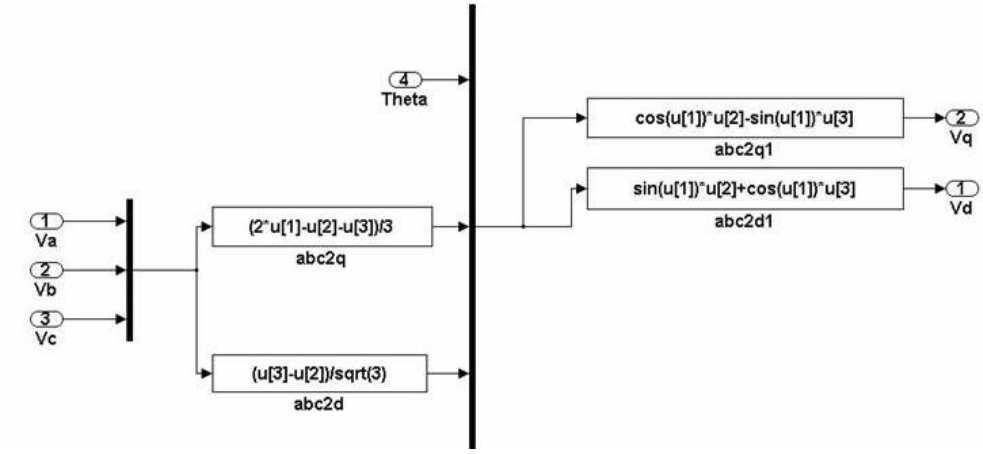

Figure A2 Schematic diagram of the transformation between the 3 and 2 phase systems in Matlab.

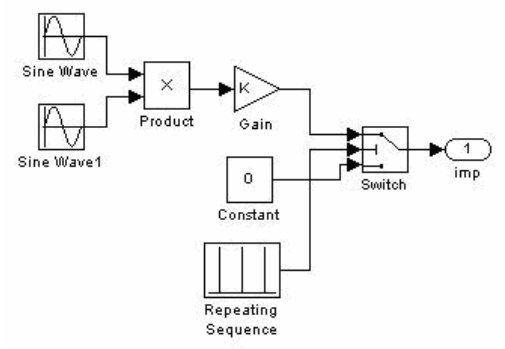

Figure A3 Impulse block.

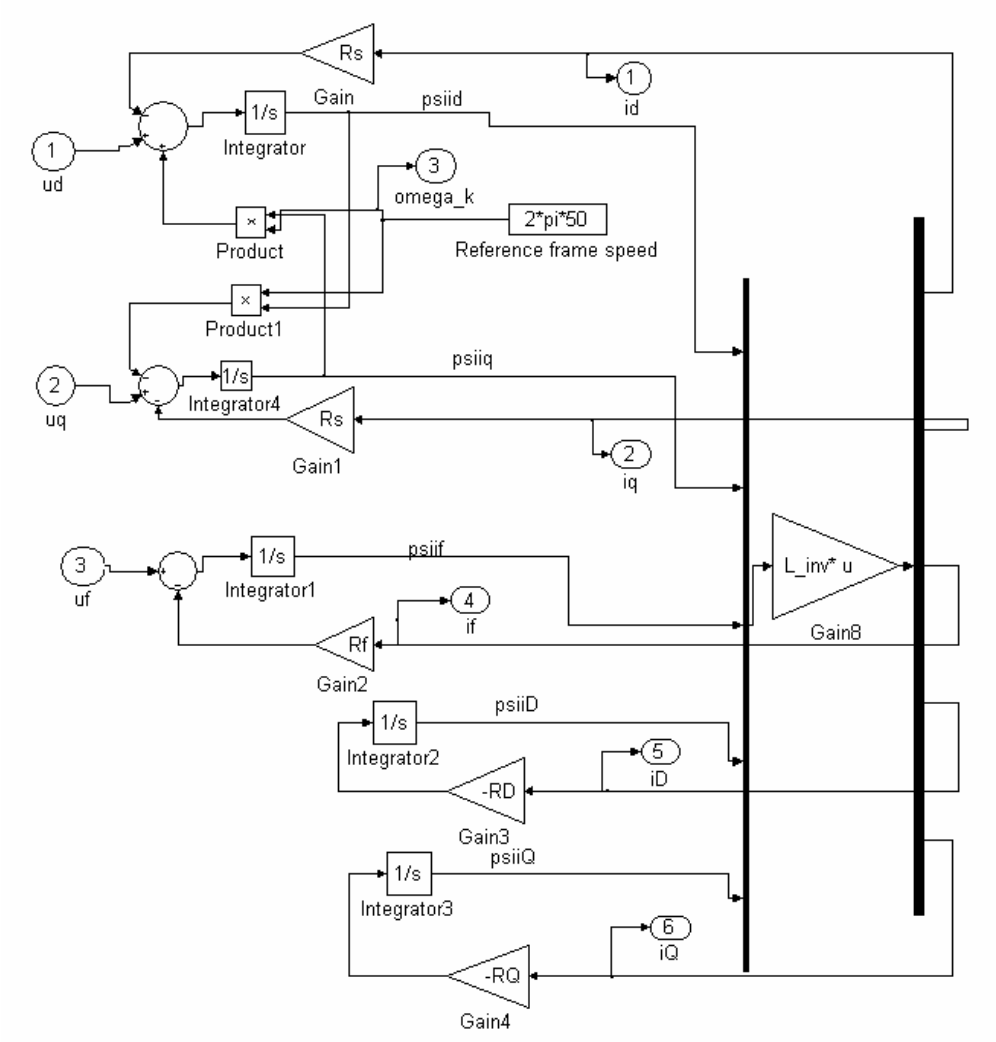

Figure A4 Synchronous machine model.

Appendix 2: Parameters of the manufacturer

Table A1 Two-axis model parameters provided by the manufacturer.

Description	Value (p. u.)
Stator resistance	0.0047
Stator leakage inductance	0.2130
Direct axis magnetizing inductance	2.4940
Quadrature axis magnetizing inductance	1.0970
Excitation winding leakage inductance	0.2270
Excitation winding resistance	0.0009
D-axis damper winding leakage inductance	0.1397
D-axis damper winding resistance	0.0453
Q-axis damper winding leakage inductance	0.1424
Q-axis damper winding resistance	0.0279